JOURNAL OF GEOPHYSICAL RESEARCH, VOL. 112, A07214, doi:10.1029/2006JA011947, 2007

An explanation for high-frequency broadband electrostatic noise in the Earth's magnetosphere

S. Moolla,[1] R. Bharuthram,[2] S. V. Singh,[3] G. S. Lakhina,[3] and R. V. Reddy[3]

Received 30 June 2006; revised 12 March 2007; accepted 23 April 2007; published 19 July 2007.

[1] A parametric study of high-frequency nonlinear electrostatic oscillations in a magnetized plasma consisting of hot electrons, cool electrons, and cool ions has been conducted. The fluid equations have been used for each species, and the coupled system of differential equations in the rest frame of the propagating wave have been numerically solved to yield the electric field for parameters characteristic of the auroral region. The effect of the initial driving amplitude, cold and hot electron densities, propagation angle, hot electron drift, and cool electron and cool ion temperatures on the electric field structures have been investigated and, in particular, the frequency and the type of electric field structure (sinusoidal, sawtooth, or spiky). The initial driving amplitude as well as the cold and hot electron densities are shown to affect the nature (sinusoidal, sawtooth, or spiky) of the waveforms, with a transition from linear sinusoidal waveforms for low initial driving amplitude, to spiky, nonlinear waveforms for larger values of the initial driving amplitude. In addition, the drifts of the species are shown to play a crucial role in the periods of the waveforms, while the temperatures of the electron species are also shown to vary the periods of the waveforms but not as much as in the case of the drifts of the species. The results show a strong resemblance to satellite observations of the different types of broadband electrostatic noise reported, which are nonlinear, spiky structures of varying amplitude and period.

Citation: Moolla, S., R. Bharuthram, S. V. Singh, G. S. Lakhina, and R. V. Reddy (2007), An explanation for high-frequency broadband electrostatic noise in the Earth's magnetosphere, *J. Geophys. Res.*, *112*, A07214, doi:10.1029/2006JA011947.

1. Introduction

[2] Satellite observations over the past 30 years have indicated the presence of broadband electrostatic noise (BEN) in different regions of the Earth's magnetosphere [*Lakhina et al.*, 2000], such as the polar cusp region [*Gurnett and Frank*, 1978] and along auroral field lines [*Gurnett and Frank*, 1977; *Temerin et al.*, 1982; *Bostrom et al.*, 1988; *Koskinen et al.*, 1990; *Tsurutani et al.*, 1998a], in the magnetopause boundary layer [*Gurnett et al.*, 1979; *Tsurutani et al.*, 1981, 1989; *Anderson et al.*, 1982; *LaBelle and Treumann*, 1998] and in the plasma sheet boundary layer [*Matsumoto et al.*, 1994]. Several theoretical attempts have been made to explain the phenomena in terms of linear instabilities, especially for the high-frequency components [*Schriver and Ashour-Abdalla*, 1987; *Lakhina and Tsurutani*, 1999; *Singh and Lakhina*, 2001]. On the basis of the fact that BEN spectra have very short temporal durations, *Anderson et al.* [1982] deduced that the high-frequency component of BEN in the magnetosheath consists of potential structures moving past a spacecraft.

[3] Recent observations by the GEOTAIL [*Matsumoto et al.*, 1994], POLAR [*Mozer et al.*, 1997; *Franz et al.*, 1998; *Tsurutani et al.*, 1998b], and FAST [*Ergun et al.*, 1998] spacecrafts have confirmed the presence of nonlinear structures in BEN [see *Matsumoto et al.*, 1994, Figure 4; *Ergun et al.*, 1998, Figure 6]. In particular, BEN is found to have waveforms of solitary bipolar electric field pulses which are called Electrostatic Solitary Waves (ESWs) [*Matsumoto et al.*, 1994]. The nonlinear BEN waveforms do not show continuous broadband noise and are composed of bipolar pulses in most cases. The bipolar signature is characterized by solitary spikes composed of a half sinusoid-like cycle followed by a similar half cycle having the opposite sign. The GEOTAIL spacecraft has measured ESWs in the plasma sheet boundary layer [*Matsumoto et al.*, 1994] and the magnetosheath [*Kojima et al.*, 1997]. On some occasions, continuous waveforms composed of quasi-monochromatic waves with strong higher harmonic components contribute to BEN [*Matsumoto et al.*, 1994].

[4] *Kojima et al.* [1994] investigated the variation of the ESW pulse width in time (i.e., pulse duration, w) and their repetition period (i.e., duration between the pulses, T) [see *Kojima et al.*, 1994, Figure 3]. They found that even though the pulse width (w) and repetition period (T) change very quickly, their ratio w/T, is more or less constant. From this observation, they concluded that the spatial size of the solitary potentials is almost constant. In addition, they also established that the rapid variation of the ESW speed could

[1]Department of Physics, University of KwaZulu-Natal, Durban, South Africa.
[2]University of Witwatersrand, Johannesburg, South Africa.
[3]Indian Institute of Geomagnetism, Navi Mumbai, India.

0148-0227/07/2006JA011947$09.00

reflect fast variation of the ion temperature and/or the electron beam speed. They concluded that the ESW consists of isolated potential humps. *Pickett et al.* [2004] reported on measurements of isolated electrostatic structures as recorded by the Wideband Plasma Wave Receiver located on each of the four Cluster spacecrafts at $4.5-6.5R_E$. These structures exhibited isolated bipolar and tripolar waveforms.

[5] Various models have been proposed to explain the solitary pulses (for a review, see *Lakhina et al.* [2000, 2003]). Most of the theoretical models fall basically in two categories, namely: (1) the soliton/solitary wave models based on fluid equations [*Temerin et al.*, 1979; *Dubouloz et al.*, 1991a, 1991b, 1993; *Reddy and Lakhina*, 1991; *Reddy et al.*, 1992; *Berthomier et al.*, 1998, 2000; *Singh et al.*, 2001a] and (2) the BGK (Bernstein-Greene-Kruskal)/phase space holes models which are essentially kinetic in nature and in which trapped particles effects play an important role in sustaining the nonlinear structures [*Muschietti et al.*, 1999; *Krasovsky et al.*, 1997]. Particle simulations of the electron-beam instabilities have contributed significantly to understanding the generation of solitary pulses in terms of electron holes [*Omura et al.*, 1994, 1996, 1999; *Kojima et al.*, 1997, 1999; *Goldman et al.*, 1999, 2000; *Singh et al.*, 2001b; *Singh*, 2003].

[6] *Krasovsky et al.* [1997] have used a BGK analysis to theoretically describe the high-frequency ESW. Using a one-dimensional electrostatic formulation, they found an expression for the plasma response to the moving perturbation of the electrostatic potential consisting of the contributions of the resonant and nonresonant untrapped plasma electrons. Using counterstreaming electron and ion beams in a two-dimensional (2-D) computer simulation experiment, *Omura et al.* [1994] have shown that the nonlinear state of the system yields electric field structures similar to those of the ESW observed in BEN. In a later study, *Krasovsky et al.* [2004] presented possible algorithms to construct 3-D models of electron holes, as a follow up to studies related to the Geotail spacecraft in which the concept of 1-D electron phase space holes was developed as possible explanations for the nonlinear waveforms.

[7] More recently, *Reddy et al.* [2002] have used a fluid theory approach to examine nonlinear low-frequency electric field structures in an electron-ion plasma. For sufficiently large values of the driver electric field, the governing equation for the electric field, produced by a nonlinear coupling between the ion acoustic wave and ion cyclotron oscillations, is found to admit both sawtooth and spiky periodic solutions (ESWs) which are in very good agreement with the observations of *Ergun et al.* [1998].

[8] Following the approach of *Reddy et al.* [2002], *Moolla et al.* [2003] studied high-frequency nonlinear waves in the Earth's magnetosphere. They considered a three-component plasma model consisting of hot electrons, cold electrons, and cold ions. The transition from sinusoidal to sawtooth to ESWs occurred as the amplitude of the driving electric field E_0 was increased. In addition, *Moolla et al.* [2003] showed that the hot electrons were accelerated in bursts leading to rapid changes in their speeds. The work carried out in this paper is an extension of that of *Moolla et al.* [2003]. In addition, we investigate the relationship between the pulse widths and periods of the waves, as well as the effects of the propagation angle on the electric field structures. In section 2, we present the basic theory, and the numerical results are presented in section 3. Finally, our findings are summarized in section 4.

2. Basic Theory

[9] We consider a three-component, collisionless, magnetized plasma consisting of hot electrons (h), cool electrons (c), and a cool ion species (i). The external magnetic field $\mathbf{B_0}$ lies in the $x-z$ plane making an angle θ with the x-axis, i.e., $\theta = \theta(\mathbf{x}, \mathbf{B_0})$. The continuity and momentum equations for the three species are given by

$$\begin{aligned}\frac{\partial n_j}{\partial t}+\frac{\partial n_j v_{jx}}{\partial x} &= 0\,\frac{\partial v_{jx}}{\partial t}+v_{jx}\frac{\partial v_{jx}}{\partial x}+\frac{1}{n_j m_j}\frac{\partial p_j}{\partial x}\\ &= -\frac{\epsilon_j e}{m_j}\frac{\partial \phi}{\partial x}+\epsilon_j\Omega_j v_{jy}\sin\theta\frac{\partial v_{jy}}{\partial t}+v_{jx}\frac{\partial v_{jy}}{\partial x}\\ &= \epsilon_j\Omega_j v_{jz}\cos\theta-\epsilon_j\Omega_j v_{jx}\sin\theta\frac{\partial v_{jz}}{\partial t}+v_{jx}\frac{\partial v_{jz}}{\partial x}\\ &= -\epsilon_j\Omega_j v_{jy}\cos\theta, \end{aligned} \tag{1}$$

where $\Omega_j = \frac{eB_0}{m_j c}$ and $\epsilon_j = +1(-1)$ for $j = i(c, h)$, with $j = i, c, h$ for the ions, and the cool and hot electrons, respectively.

[10] The general equation of state for the three species is given by

$$\frac{\partial p_j}{\partial t}+v_{jx}\frac{\partial p_j}{\partial x}+3p_j\frac{\partial v_{jx}}{\partial x}=0, \tag{2}$$

where p_j is the pressure of the jth species, and we assume adiabatic compression ($\gamma = (2 + N)/N = 3$, where $N = 1$ implies one degree of freedom). The system of equations is closed with the Poisson equation

$$\frac{\partial^2\phi}{\partial x^2}=-\frac{e}{\epsilon_0}(n_i-n_c-n_h). \tag{3}$$

In the above equations, n_j is the density of the jth species, v_{jx}, v_{jy}, v_{jz} are the velocities of the jth species in the x, y, and z directions, respectively, and Ω_j is the electron (ion) cyclotron frequency for $j = e$ (i). We allow spatial variation only in the x-direction.

2.1. Linear Analysis

[11] The above set of equations may be linearized and combined to yield the general dispersion relation:

$$\begin{aligned}\omega^2 = &\frac{\omega_{pi}^2\left(\omega^2-\Omega_i^2\cos^2\theta\right)}{\omega^2-\Omega_i^2-\left(3k^2v_{ti}^2/\omega^2\right)\left(\omega^2-\Omega_i^2\cos^2\theta\right)}\\ &+\frac{\omega_{pc}^2\left(\omega^2-\Omega_e^2\cos^2\theta\right)}{\omega^2-\Omega_e^2-\left(3k^2v_{tc}^2/\omega^2\right)\left(\omega^2-\Omega_e^2\cos^2\theta\right)}\\ &+\frac{\omega_{ph}^2\left(\omega^2-\Omega_e^2\cos^2\theta\right)}{\omega^2-\Omega_e^2-\left(3k^2v_{th}^2/\omega^2\right)\left(\omega^2-\Omega_e^2\cos^2\theta\right)}, \end{aligned} \tag{4}$$

where $\omega_{pi,c,h}$ are the ion, cool electron, and hot electron plasma frequencies, respectively, such that $\omega_{pj} = \sqrt{4\pi n_{0j}e^2/m_j}$; and $v_{ti,c,h}$ are the cool ion, cool electron, and hot electron thermal velocities, respectively, with $v_{ti} = \sqrt{T_i/m_i}$, $v_{tc} = \sqrt{T_c/m_e}$, and $v_{th} = \sqrt{T_h/m_e}$, where T_j is the

temperature of the jth species with $T_h \gg T_c$, T_i. For high-frequency waves, one may neglect the ion motion. Then, in the limits $\omega/k \ll v_{th}$ and $\omega/k \gg v_{tc}$, the dispersion relation (7) yields [*Mace and Hellberg*, 1993]

$$\omega^2 = \frac{1}{2}\left(\omega_s^2 + \Omega_e^2\cos^2\theta\right)\left[1 \pm \sqrt{1 - \frac{4\omega_s^2\Omega_e^2\cos^2\theta}{\left(\omega_s^2 + \Omega_e^2\cos^2\theta\right)^2}}\right], \quad (5)$$

where $\omega_s = \sqrt{3}\omega_{pc}k\lambda_{Dh}\cos\theta$, and $\lambda_{Dh} = \sqrt{T_h/4\pi n_{0h}e^2}$ is the hot electron Debye length. The solution of equation (8) yields two modes: the positive sign gives the electron cyclotron mode, $\omega_+ = \Omega_e\cos\theta$, and the negative sign gives the electron acoustic mode, $\omega- = \omega_s$.

2.2. Nonlinear Analysis

[12] In the nonlinear regime, the ECW and the EAW may couple through the convective terms in equations (2)–(4). For the analysis, we transform to a stationary frame $s = (x - Vt)/(V/\Omega_e)$ and normalize v, t, x and ϕ with respect to v_{th}, Ω_e^{-1}, $\rho_e = v_{th}/\Omega_e$, and T_h/e, respectively. In equations (1)–(4), we replace $\frac{\partial}{\partial t}$ by $-\Omega_e\frac{\partial}{\partial s}$ and $\frac{\partial}{\partial x}$ by $(\Omega_e/V)\frac{\partial}{\partial s}$. In addition, we define $E = -\frac{\partial\psi}{\partial s}$, where $\psi = e\phi/T_h$. The evolution of the plasma is then determined by the following set of nonlinear, first-order differential equations:

$$\frac{\partial\psi}{\partial s} = -E \quad (6)$$

$$\frac{\partial E}{\partial s} = -R_e^2M^2(n_{in} - n_{cn} - n_{hn}) \quad (7)$$

$$\frac{\partial n_{in}}{\partial s} = \frac{\frac{m_e}{m_i}\left[E - Mv_{iyn}\sin\theta\right]n_{in}^3}{(M-\delta_i)^2 - 3\frac{T_i}{T_h}\frac{m_e}{m_i}p_{in}n_{in}} \quad (8)$$

$$\frac{\partial v_{iyn}}{\partial s} = \frac{m_e}{m_i}n_{in}\frac{M}{(M-\delta_i)}\left[\left(M - \frac{(M-\delta_i)}{n_{in}}\right)\sin\theta - v_{izn}\cos\theta\right] \quad (9)$$

$$\frac{\partial v_{izn}}{\partial s} = \frac{m_e}{m_i}n_{in}\frac{Mv_{iyn}}{(M-\delta_i)}\cos\theta \quad (10)$$

$$\frac{\partial p_{in}}{\partial s} = \frac{3p_{in}}{n_{in}}\frac{\frac{m_e}{m_i}\left[E - Mv_{iyn}\sin\theta\right]n_{in}^3}{(M-\delta_i)^2 - 3\frac{T_i}{T_h}\frac{m_e}{m_i}p_{in}n_{in}} \quad (11)$$

$$\frac{\partial n_{cn}}{\partial s}\frac{n_{cn}^3\left[-E + Mv_{cyn}\sin\theta\right]}{\left(\frac{n_{0c}}{n_0}\right)^2(M-\delta_c)^2 - 3\frac{T_c}{T_h}p_{cn}n_{cn}} \quad (12)$$

$$\frac{\partial v_{cyn}}{\partial s} = \frac{Mn_{cn}}{(M-\delta_c)}\frac{n_0}{n_{0c}}\left[-\left(M - \frac{(M-\delta_c)}{n_{cn}}\frac{n_{0c}}{n_0}\right)\sin\theta + v_{czn}\cos\theta\right] \quad (13)$$

$$\frac{\partial v_{czn}}{\partial s} = -n_{cn}\frac{Mv_{cyn}}{(M-\delta_c)}\cos\theta\frac{n_0}{n_{0c}} \quad (14)$$

$$\frac{\partial p_{cn}}{\partial s} = \frac{3p_{cn}n_{cn}^2\left(Mv_{cyn}\sin\theta - E\right)}{(M-\delta_c)^2\left(\frac{n_{0c}}{n_0}\right)^2 - 3\frac{T_c}{T_h}p_{cn}n_{cn}} \quad (15)$$

$$\frac{\partial p_{hn}}{\partial s} = \frac{3p_{hn}n_{hn}^2\left(Mv_{hyn}\sin\theta - E\right)}{(M-\delta_h)^2\left(\frac{n_{0h}}{n_0}\right)^2 - 3p_{hn}n_{hn}} \quad (16)$$

$$\frac{\partial n_{hn}}{\partial s} = \frac{n_{hn}^3\left(Mv_{hyn}\sin\theta - E\right)}{(M-\delta_h)^2\left(\frac{n_{0h}}{n_0}\right)^2 - 3p_{hn}n_{hn}} \quad (17)$$

$$\frac{\partial v_{hyn}}{\partial s} = \frac{Mn_{hn}}{(M-\delta_h)}\frac{n_0}{n_{0h}}\left[-\left(M - \frac{(M-\delta_h)}{n_{hn}}\frac{n_{0h}}{n_0}\right)\sin\theta + v_{hzn}\cos\theta\right] \quad (18)$$

$$\frac{\partial v_{hzn}}{\partial s} = -\frac{n_0}{n_{0h}}n_{hn}\frac{Mv_{hyn}}{(M-\delta_h)}\cos\theta. \quad (19)$$

In equations (9)–(20), $E_0 = \frac{\partial\psi}{\partial s}$ at $s = 0$ is the initial (driving) electric field amplitude, $R_e = \omega_{pe}/\Omega_e$, where $\omega_{pe} = (4\pi n_0e^2/m_e)^{1/2}$ is the total electron plasma frequency, $M = V/v_{th}$ is the Mach number, $n_{0c}(n_{0h})$ is the equilibrium density of the cool (hot) electrons with $n_{0c} + n_{0h} = n_{i0} = n_0$, and $\delta_j = v_{0j}/v_{th}$ is the normalized flow velocity of species j at $s = 0$. The additional subscript "n" for the plasma parameters indicates normalized quantities.

3. Numerical Results

[13] Equations (9)–(20) are solved using the Runge-Kutta (RK) technique [*Press et al.*, 1996]. The method involves providing initial values to plasma parameters and using the RK-4 subroutine [*Press et al.*, 1996] to advance the functions with a suitable step length. It is important to note that we plot the actual normalized electric field $E_{actual} = -(1/M)\frac{\partial\psi}{\partial s}$. The results are discussed in the next section.

3.1. Effect of the Driving Electric Field Amplitude, E_0

[14] In Figures 1a, 1b, 1c, and 1d, for fixed $M = 2.5$, we vary E_0, the initial driving electric field. Here $\theta = 2°$, so that the wave propagation is essentially parallel to $\mathbf{B_0}$. This value is consistent with the experimental observations of *Ergun et al.* [1998], who indicated spiky structures for parallel wave propagation. Also, $n_{0c}/n_0 = 0.5$, $\delta_i = \delta_c = \delta_h = 0.0$ (i.e., all species are initially stationary), $T_c/T_h = 0.05$ and $T_i/T_h = 0.0$. It can be seen from the figures that as E_0 increases, the electric field evolves from a sinusoidal wave to a sawtooth structure. For larger values of E_0, the wave becomes a periodic structure of bipolar pulses, which are very similar to the high-frequency electrostatic solitary waves (ESWs) observed in the BEN in different regions of the magneto-

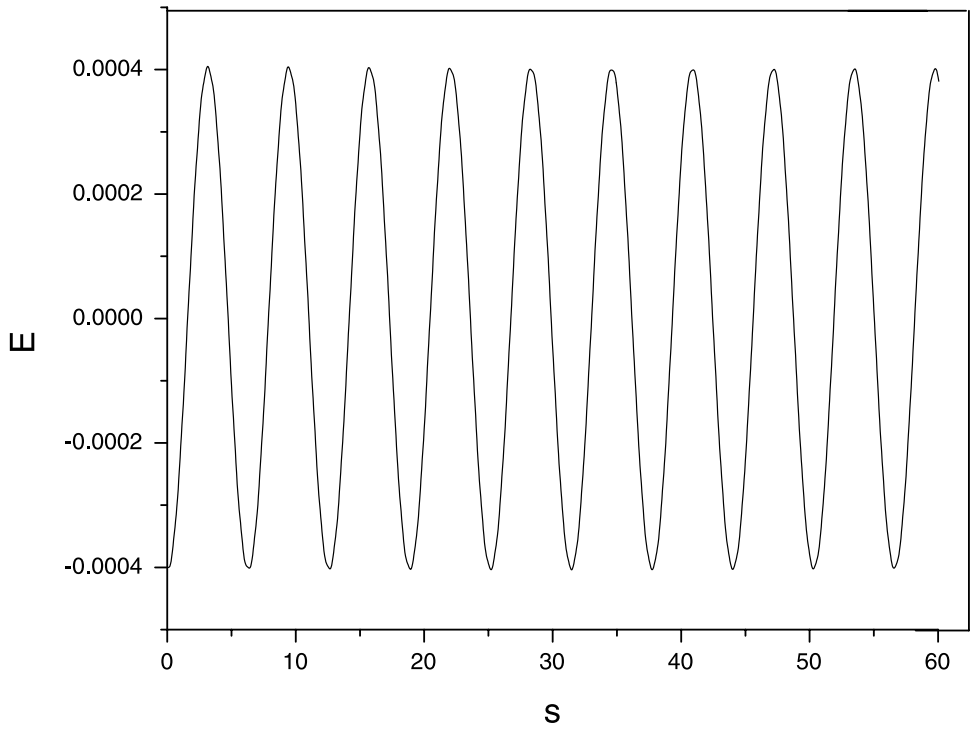

Figure 1a. Numerical solution of the electric field (sinusoidal waveform) for the parameters $\theta = 2°$, $M = 2.5$, $n_{0c}/n_0 = 0.5$, $R_e = 1.0$, $\delta_i = \delta_c = \delta_h = 0.0$, $T_c/T_h = 0.05$, $T_i/T_h = 0.0$, and $E_0 = 0.001$. The period, T_w of the wave is $0.95\tau_{ce}$ (frequency $f_w = 1.04f_{ce}$).

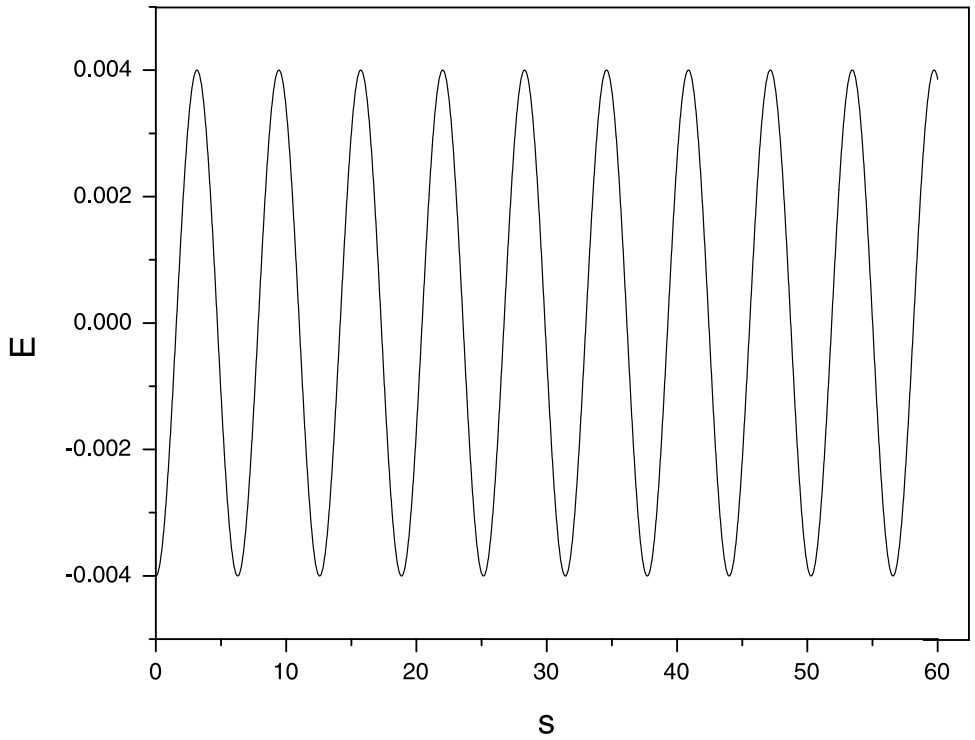

Figure 1b. Numerical solution of the electric field (sinusoidal waveform) for the parameters $\theta = 2°$, $M = 2.5$, $n_{0c}/n_0 = 0.5$, $R_e = 1.0$, $\delta_i = \delta_c = \delta_h = 0.0$, $T_c/T_h = 0.05$, $T_i/T_h = 0.0$, and $E_0 = 0.01$. The period, T_w of the wave is $0.97\tau_{ce}$ (frequency $f_w = 1.03f_{ce}$).

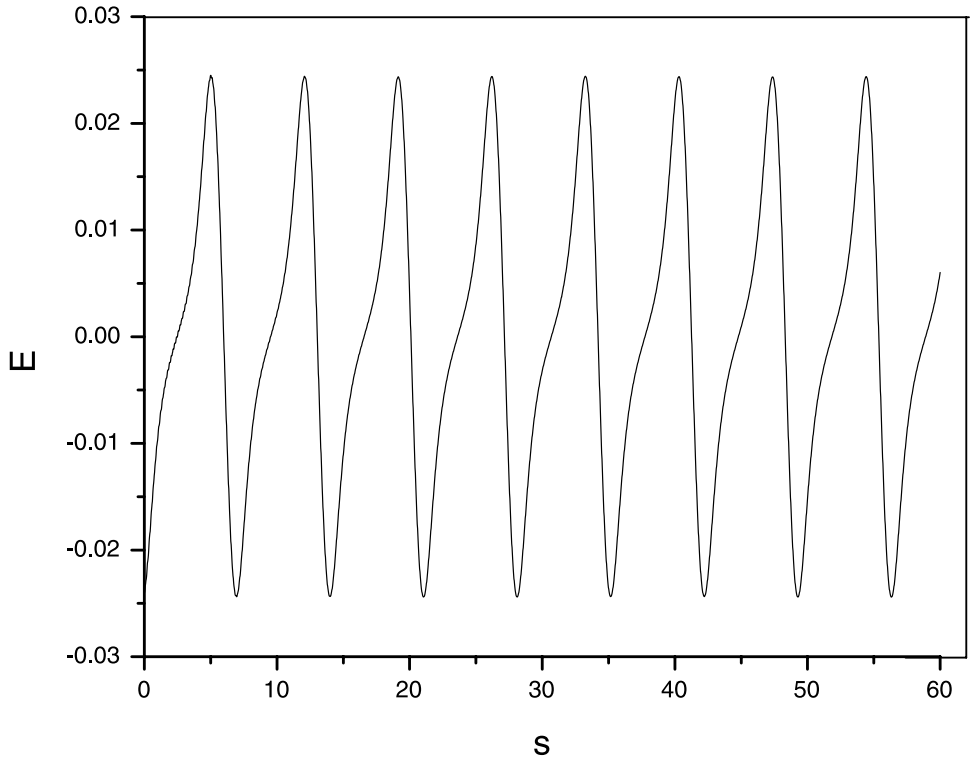

Figure 1c. Numerical solution of the electric field (sawtooth waveform) for the parameters $\theta = 2°$, $M = 2.5$, $n_{0c}/n_0 = 0.5$, $R_e = 1.0$, $\delta_i = \delta_c = \delta_h = 0.0$, $T_c/T_h = 0.05$, $T_i/T_h = 0.0$, and $E_0 = 0.06$. The period, T_w of the wave is $1.14\tau_{ce}$ (frequency $f_w = 0.88 f_{ce}$).

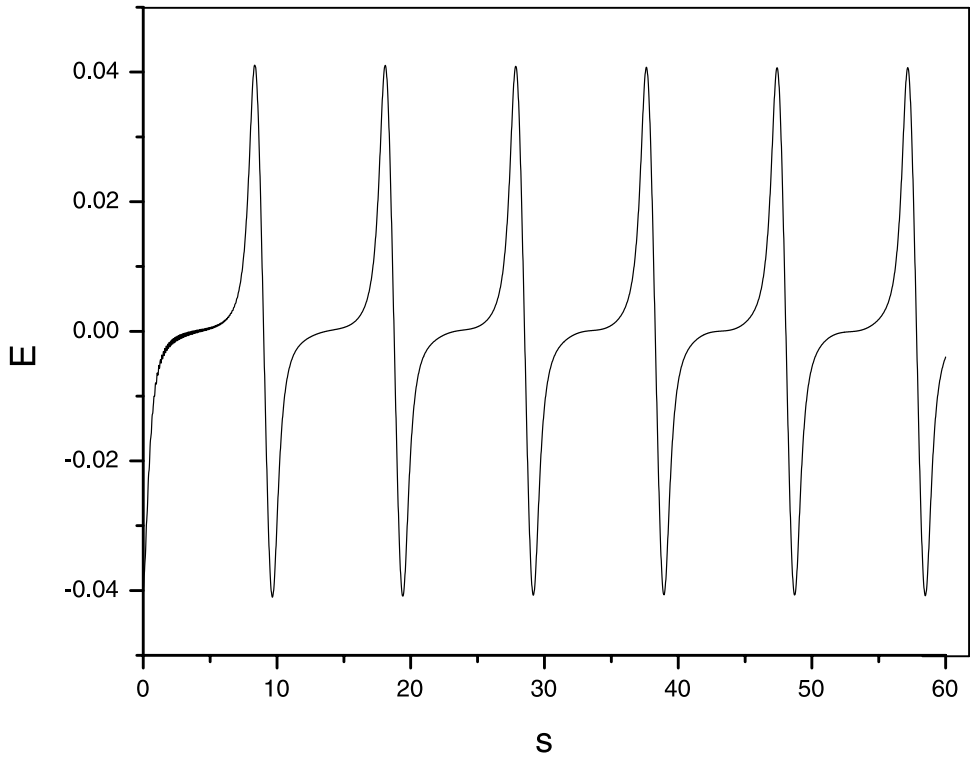

Figure 1d. Numerical solution of the electric field (bipolar waveform) for the parameters $\theta = 2°$, $M = 2.5$, $n_{0c}/n_0 = 0.5$, $R_e = 1.0$, $\delta_i = \delta_c = \delta_h = 0.0$, $T_c/T_h = 0.05$, $T_i/T_h = 0.0$, and $E_0 = 0.10$. The period, T_w of the wave is $1.59\tau_{ce}$ (frequency $f_w = 0.63 f_{ce}$).

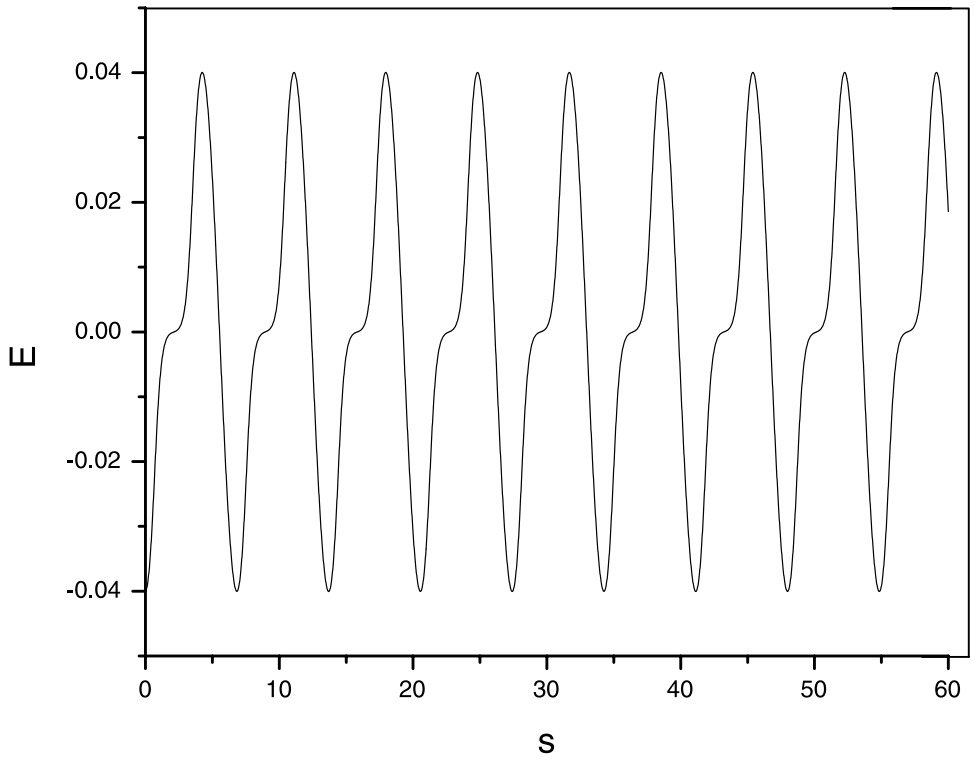

Figure 2a. ESW with $M = 2.5$, $\theta = 2°$, $\delta_i = \delta_c = \delta_h = 0.0$, $R_e = 1.0$, $T_c/T_h = 0.05$, $T_i/T_h = 0.0$, $E_0 = 0.10$, and $n_{0c}/n_0 = 0.2$. The period, T_w of the wave is $1.14\tau_{ce}$ (frequency $f_w = 0.88f_{ce}$).

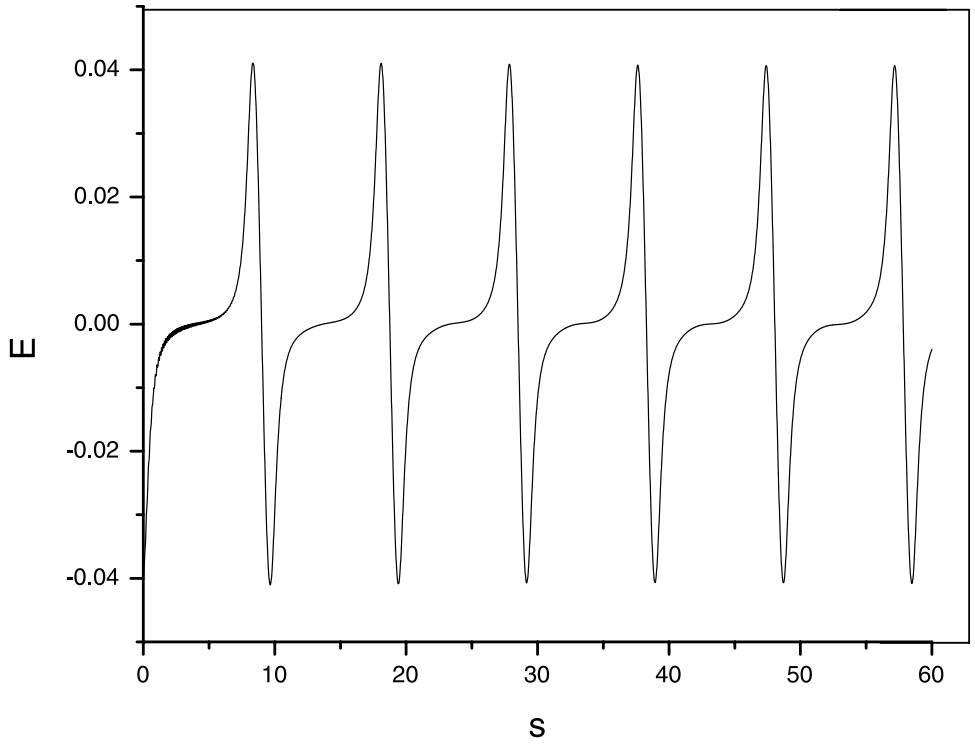

Figure 2b. ESW with $M = 2.5$, $\theta = 2°$, $\delta_i = \delta_c = \delta_h = 0.0$, $R_e = 1.0$, $T_c/T_h = 0.05$, $T_i/T_h = 0.0$, $E_0 = 0.10$, and $n_{0c}/n_0 = 0.5$. The period, T_w of the wave is $1.59\tau_{ce}$ (frequency $f_w = 0.63f_{ce}$).

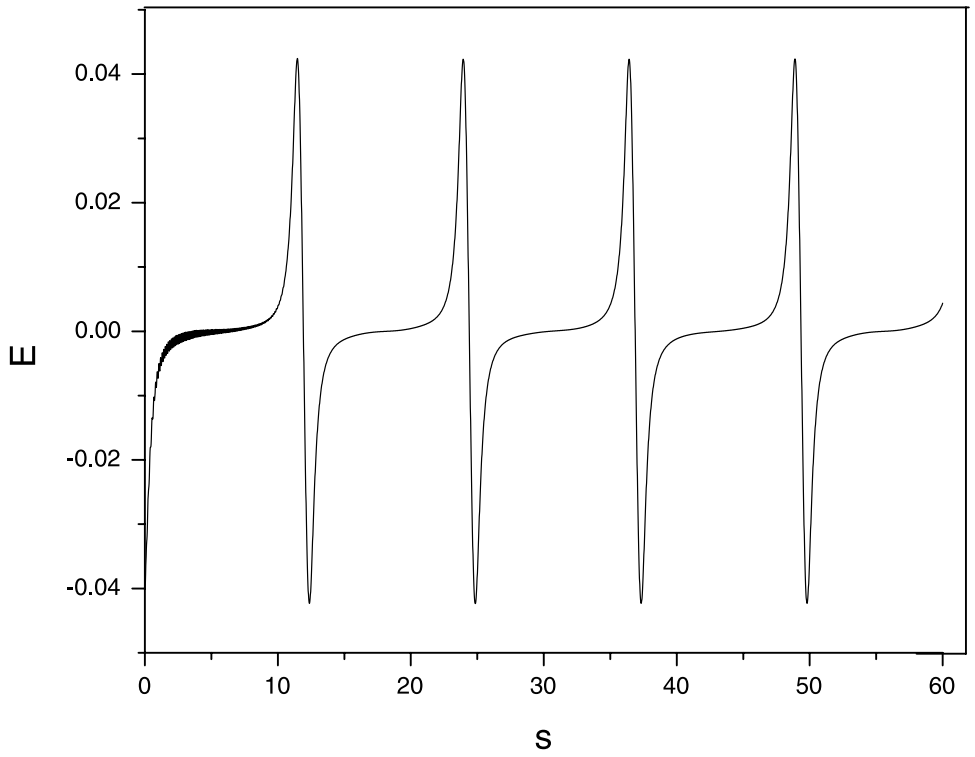

Figure 2c. ESW with $M = 2.5$, $\theta = 2°$, $\delta_i = \delta_c = \delta_h = 0.0$, $R_e = 1.0$, $T_c/T_h = 0.05$, $T_i/T_h = 0.0$, $E_0 = 0.10$, and $n_{0c}/n_0 = 0.8$. The period, T_w of the wave is $2.05\tau_{ce}$ (frequency $f_w = 0.49f_{ce}$).

sphere [*Franz et al.*, 1998; *Matsumoto et al.*, 1994]. TYPE A BEN consists of single, isolated pulses, and these pulses are uniform with no distortion. TYPE C BEN, on the other hand, consists of pulses that are distorted, resulting in double-humped structures. Hence Figures 1a–1d correspond to TYPE A BEN.

[15] As discussed previously by *Moolla et al.* [2003], for $\Delta x = 0$, $\Delta s = |\Omega_e \Delta t|$. Then for the linear wave ($E_0 = 0.001$, as in Figure 1a) one finds $\omega = 1.04\Omega_e$, which represents the electron cyclotron wave (ECW). As E_0 increases, the period of the nonlinear structures increases. Consequently, the frequency decreases with $\omega = 1.03\Omega_e$ for $E_0 = 0.01$, $\omega = 0.88\Omega_e$ for $E_0 = 0.06$, and $\omega = 0.63\Omega_e$ for $E_0 = 0.10$ (Figure 1d). This decrease can be expressed in terms of the electron cyclotron period, $\tau_{ce} = \frac{2\pi}{\Omega_{ce}}$. For $E_0 = 0.01$, the period is $0.97\tau_{ce}$. For $E_0 = 0.06$ and 0.10, the period increases to $1.14\tau_{ce}$ and $1.59\tau_{ce}$, respectively.

3.2. Effect of Cold and Hot Electron Densities

[16] The effect of a variation of the relative densities of the cold and hot electrons on the electric field structures are shown in Figures 2a–2c. In each of these figures, the fixed parameters are $M = 2.5$, $E_0 = 0.10$, $\theta = 2°$, $\delta_i = \delta_c = \delta_h = 0.0$, $R_e = 1.0$, $T_c/T_h = 0.05$, and $T_i/T_h = 0.0$. It was found that as n_{0c}/n_0 increases from 0.2 (Figure 2a) to 0.8 (Figure 2c), the electric field evolves into to a nonlinear, spiky structure. *Schriver and Ashour-Abdalla* [1987] have shown that the growth rate of the high-frequency electron acoustic instability in the BEN for typical plasma sheet boundary layer parameters increases as n_{0c}/n_0 increases. Therefore as n_{0c}/n_0 increases, nonlinearity is enhanced, which is consistent with our findings. Thus the cold electron density plays a critical role in the linear and nonlinear stability of the waves. In terms of the periods of the ESWs, for $n_{0c}/n_0 = 0.8$, the period is $2.05\tau_{ce}$, dropping to about $1.14\tau_{ce}$ for $n_{0c}/n_0 = 0.2$. Since all the periods are greater than $1.0\tau_{ce}$, we tentatively identify the mode as the electron acoustic wave (EAW). However, the possibility that the nonlinear frequency shifts, arising due to coupling between the electron cyclotron and electron acoustic modes, being responsible for a change in the time period of the mode can not be ruled out.

3.3. Effect of the Cool Electron Drift

[17] Next, we investigate the effect of a drifting cool electron component, as seen in Figures 3a–3e. The parameters kept fixed are $M = 2.5$, $E_0 = 0.10$, $\theta = 2°$, $n_{0c}/n_0 = 0.5$, $\delta_i = \delta_h = 0.0$, $R_e = 1.0$, $T_c/T_h = 0.05$, and $T_i/T_h = 0.0$. In our nonlinear set of equations, the cool electron drift is characterized by $\delta_c = v_{0c}/v_{th}$. It is noted that $\delta_c < 0$, as in Figures 3a and 3b, ($\delta_c > 0$, as in Figure 3c and 3d) imply antiparallel (parallel) to the external magnetic field B_0 cool electron drift. We observe that in moving from anti-parallel to parallel cool electron drift, the frequency of the ESWs decreases. As one moves from an antiparallel cool electron drift with $\delta_c = -0.5$, to a parallel drift with $\delta_c = 0.5$, the period of the ESW increases from $1.25\tau_{ce}$ to $2.62\tau_{ce}$ (in both cases frequency $\omega < \Omega_e$ which represents the EAW). Similar studies for the drifts of the cool ions showed no effect on the period of the ESW. The variation of the repetition period of the ESWs observed by the GEOTAIL spacecraft [see *Kojima et al.*, 1994, Figure 3] could therefore imply that the cool electrons are accelerated in bursts leading to a rapid variation in the electron-beam speed, with a subsequent change in the period of the ESWs.

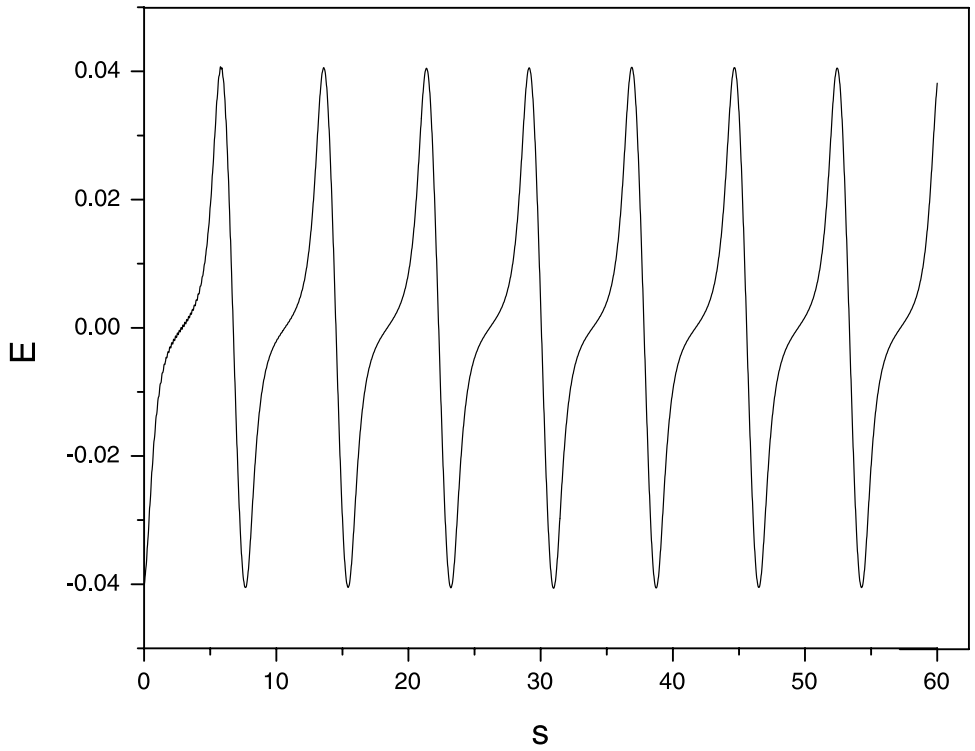

Figure 3a. ESW for varying cool electron drifts (with respect to $\mathbf{B_0}$) with $M = 2.5$, $E_0 = 0.10$, $\theta = 2°$, $\delta_i = \delta_h = 0.0$, $R_e = 1.0$, $n_{0c}/n_0 = 0.5$, $T_c/T_h = 0.05$, $T_i/T_h = 0.0$, and $\delta_c = -0.5$ (antiparallel). The period, T_w of the wave is $1.25\tau_{ce}$ (frequency $f_w = 0.80 f_{ce}$).

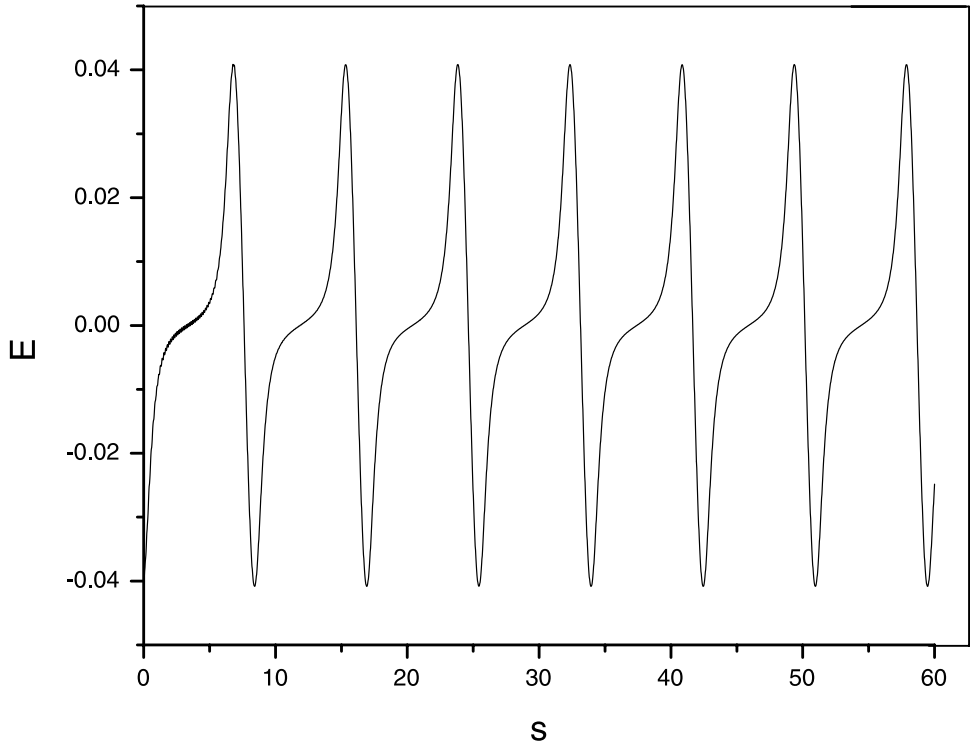

Figure 3b. ESW for varying cool electron drifts (with respect to $\mathbf{B_0}$) with $M = 2.5$, $E_0 = 0.10$, $\theta = 2°$, $\delta_i = \delta_h = 0.0$, $R_e = 1.0$, $n_{0c}/n_0 = 0.5$, $T_c/T_h = 0.05$, $T_i/T_h = 0.0$, and $\delta_c = -0.25$ (antiparallel). The period, T_w of the wave is $1.36\tau_{ce}$ (frequency $f_w = 0.74 f_{ce}$).

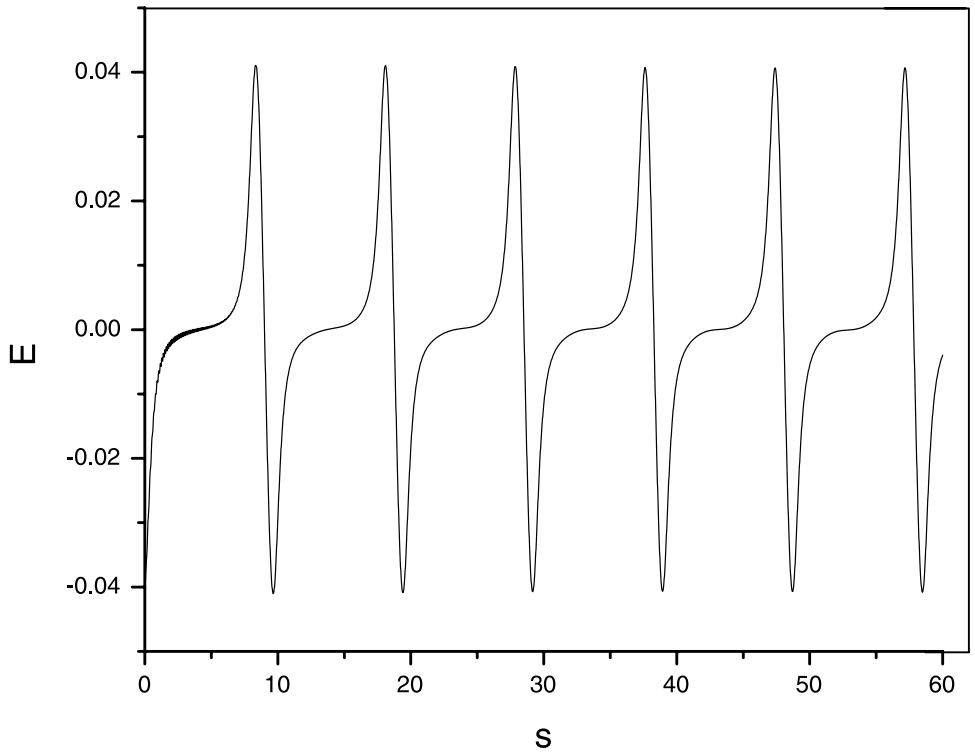

Figure 3c. ESW for varying cool electron drifts (with respect to $\mathbf{B_0}$) with $M = 2.5$, $E_0 = 0.10$, $\theta = 2°$, $\delta_i = \delta_h = 0.0$, $R_e = 1.0$, $n_{0c}/n_0 = 0.5$, $T_c/T_h = 0.05$, $T_i/T_h = 0.0$, and $\delta_c = 0.0$ (no drift). The period, T_w of the wave is $1.59\tau_{ce}$ (frequency $f_w = 0.63f_{ce}$).

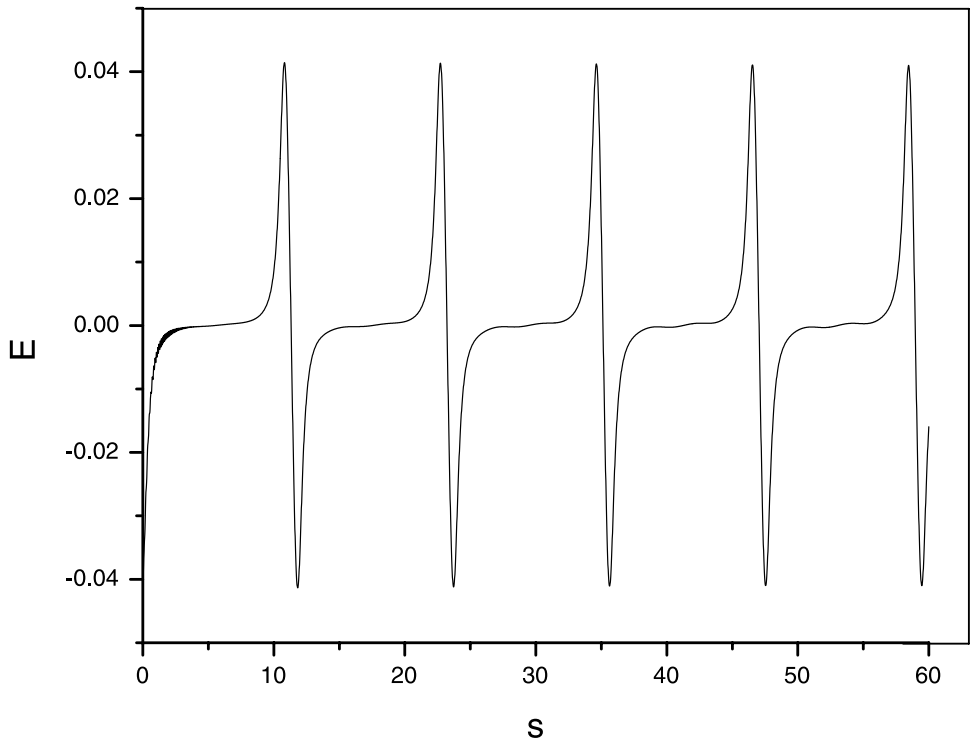

Figure 3d. ESW for varying cool electron drifts (with respect to $\mathbf{B_0}$) with $M = 2.5$, $E_0 = 0.10$, $\theta = 2°$, $\delta_i = \delta_h = 0.0$, $R_e = 1.0$, $n_{0c}/n_0 = 0.5$, $T_c/T_h = 0.05$, $T_i/T_h = 0.0$, and $\delta_c = 0.25$ (parallel). The period, T_w of the wave is $1.93\tau_{ce}$ (frequency $f_w = 0.52f_{ce}$).

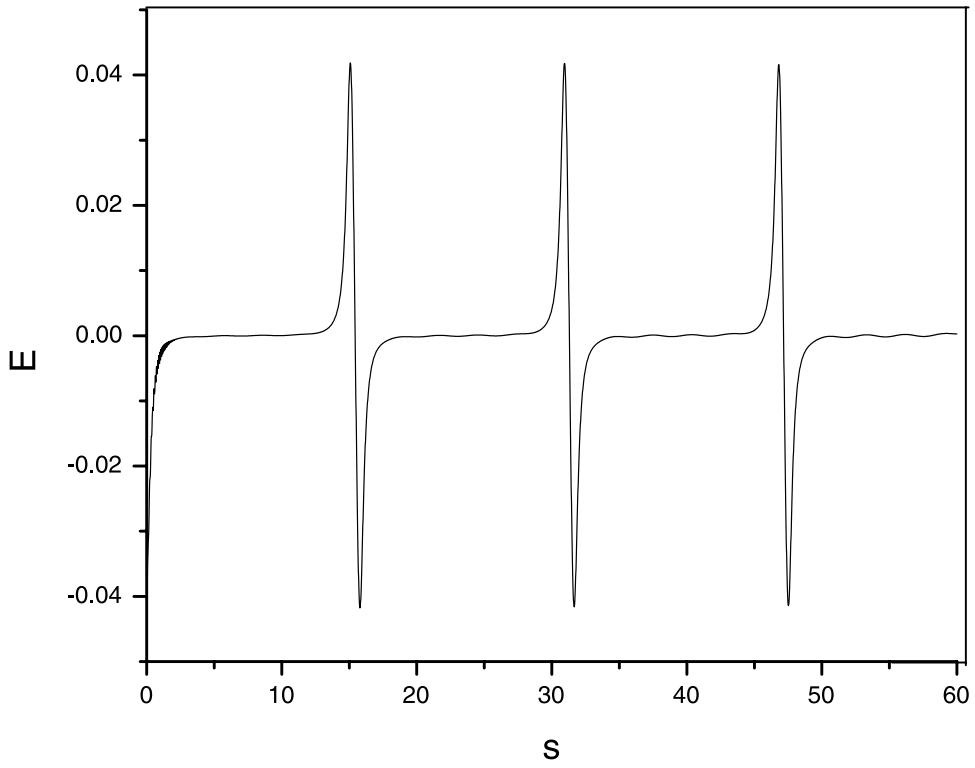

Figure 3e. ESW for varying cool electron drifts (with respect to $\mathbf{B_0}$) with $M = 2.5$, $E_0 = 0.10$, $\theta = 2°$, $\delta_i = \delta_h = 0.0$, $R_e = 1.0$, $n_{0c}/n_0 = 0.5$, $T_c/T_h = 0.05$, $T_i/T_h = 0.0$, and $\delta_c = 0.5$ (parallel). The period, T_w of the wave is $2.62\tau_{ce}$ (frequency $f_w = 0.38 f_{ce}$).

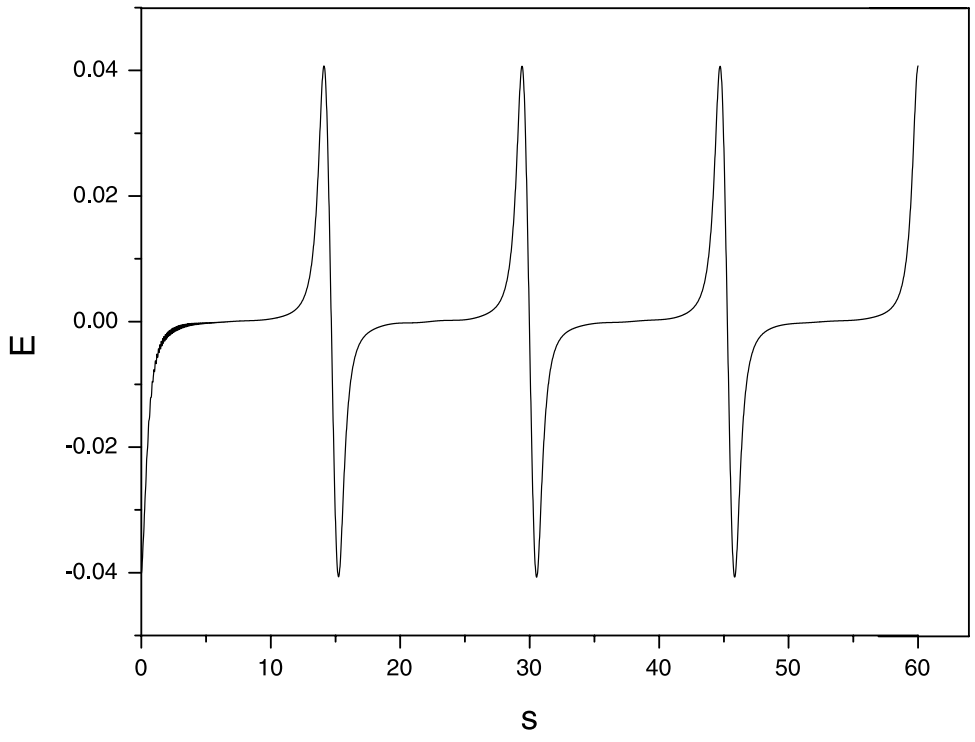

Figure 4a. ESW for varying hot electron drifts (with respect to $\mathbf{B_0}$) with $M = 2.5$, $E_0 = 0.10$, $\theta = 2°$, $\delta_i = \delta_c = 0.0$, $R_e = 1.0$, $n_{0c}/n_0 = 0.5$, $T_c/T_h = 0.05$, $T_i/T_h = 0.0$, and $\delta_h = -0.5$ (antiparallel). The period, T_w of the wave is $2.39\tau_{ce}$ (frequency $f_w = 0.42 f_{ce}$).

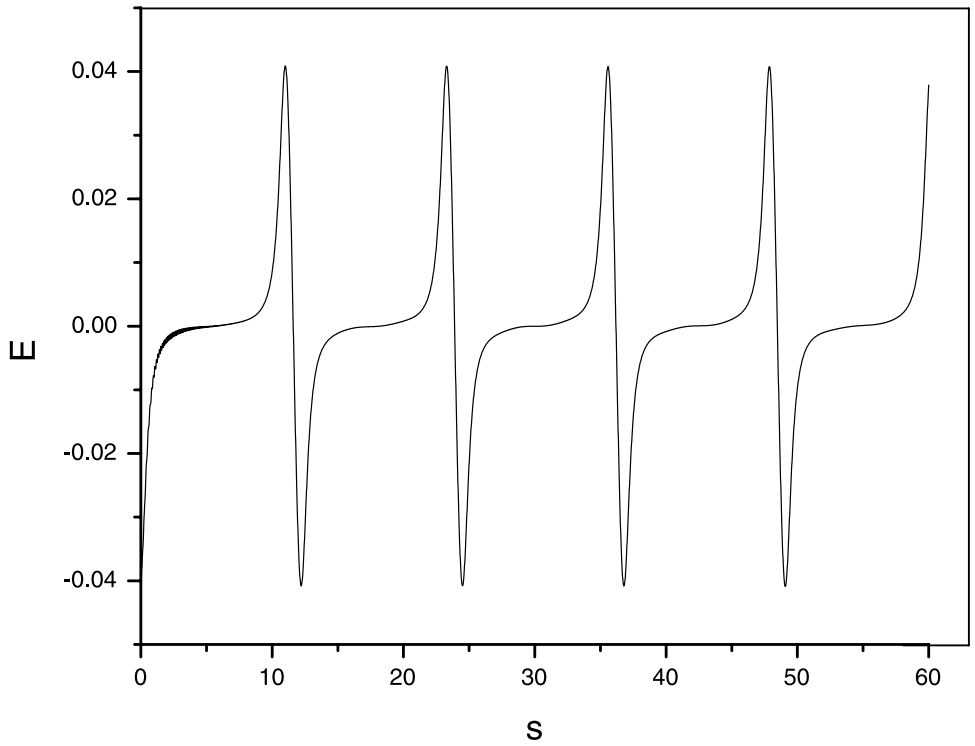

Figure 4b. ESW for varying hot electron drifts (with respect to $\mathbf{B_0}$) with $M = 2.5$, $E_0 = 0.10$, $\theta = 2°$, $\delta_i = \delta_c = 0.0$, $R_e = 1.0$, $n_{0c}/n_0 = 0.5$, $T_c/T_h = 0.05$, $T_i/T_h = 0.0$, and $\delta_h = -0.25$ (antiparallel). The period, T_w of the wave is $1.93\tau_{ce}$ (frequency $f_w = 0.52f_{ce}$).

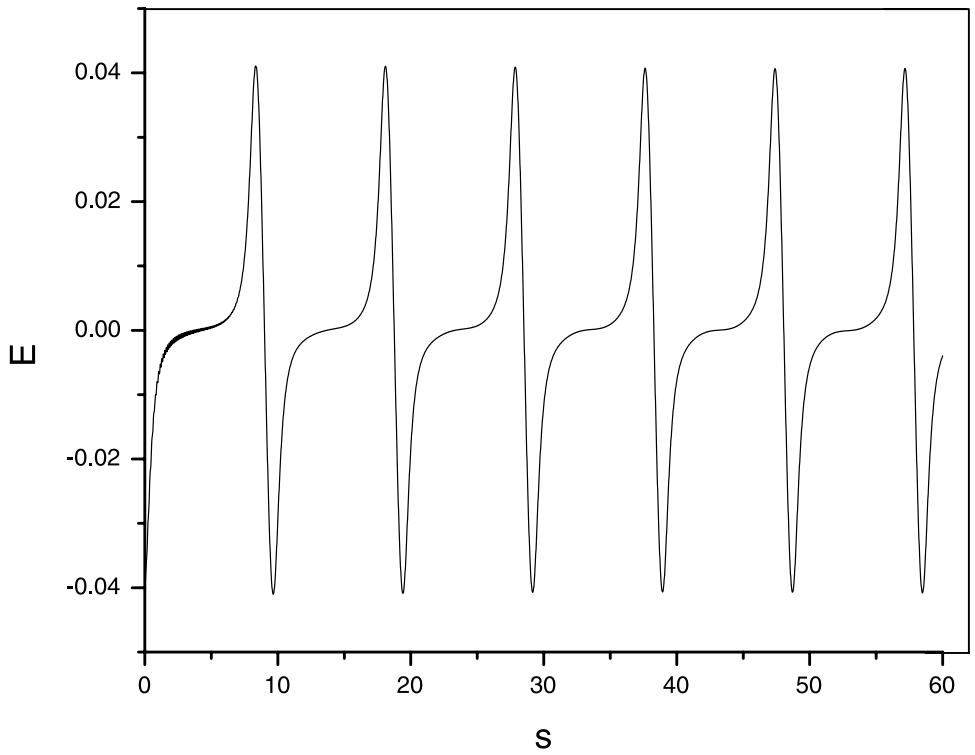

Figure 4c. ESW for varying hot electron drifts (with respect to $\mathbf{B_0}$) with $M = 2.5$, $E_0 = 0.10$, $\theta = 2°$, $\delta_i = \delta_c = 0.0$, $R_e = 1.0$, $n_{0c}/n_0 = 0.5$, $T_c/T_h = 0.05$, $T_i/T_h = 0.0$, and $\delta_h = 0.0$ (no drift). The period, T_w of the wave is $1.59\tau_{ce}$ (frequency $f_w = 0.63f_{ce}$).

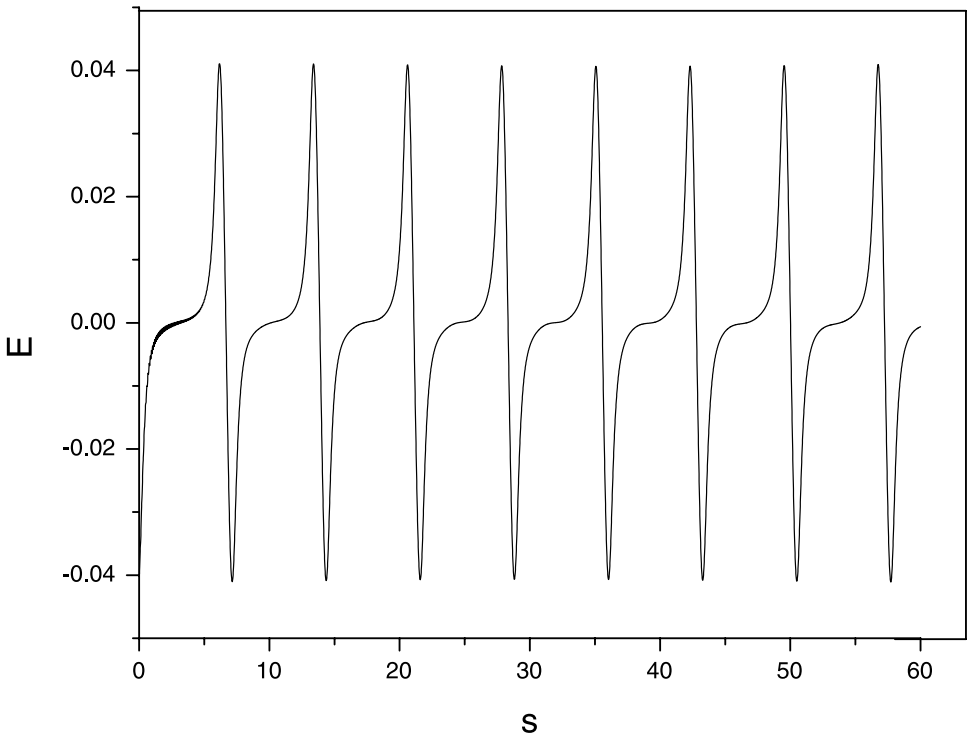

Figure 4d. ESW for varying hot electron drifts (with respect to $\mathbf{B_0}$) with $M = 2.5$, $E_0 = 0.10$, $\theta = 2°$, $\delta_i = \delta_c = 0.0$, $R_e = 1.0$, $n_{0c}/n_0 = 0.5$, $T_c/T_h = 0.05$, $T_i/T_h = 0.0$, and $\delta_h = 0.25$ (parallel). The period, T_w of the wave is $1.14\tau_{ce}$ (frequency $f_w = 0.88f_{ce}$).

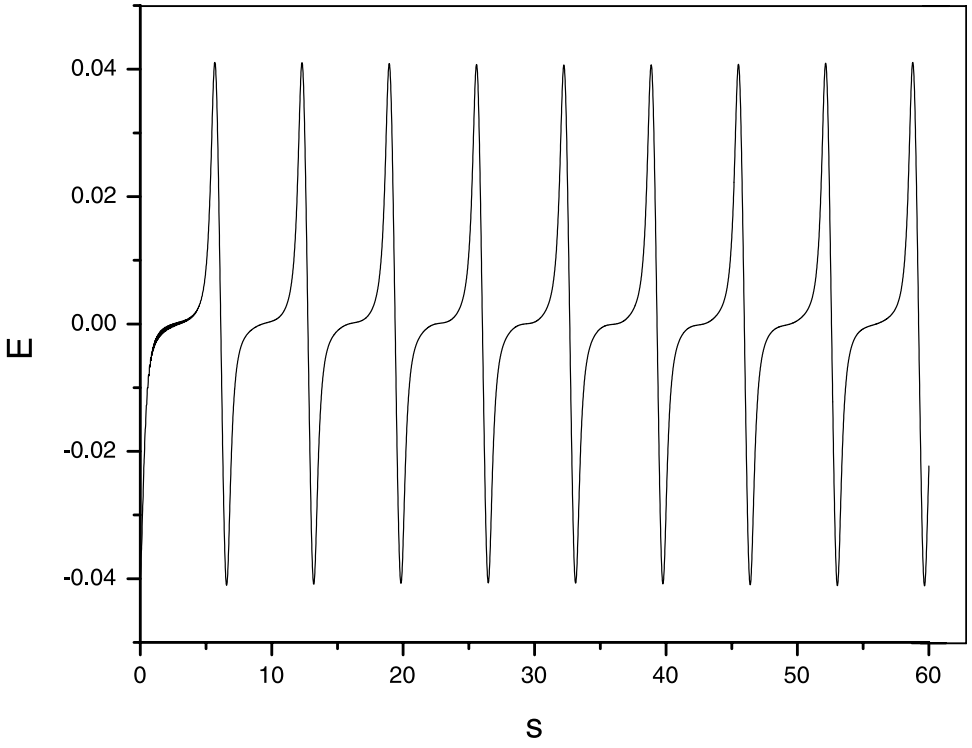

Figure 4e. ESW for varying hot electron drifts (with respect to $\mathbf{B_0}$) with $M = 2.5$, $E_0 = 0.10$, $\theta = 2^o$, $\delta_i = \delta_c = 0.0$, $R_e = 1.0$, $n_{0c}/n_0 = 0.5$, $T_c/T_h = 0.05$, $T_i/T_h = 0.0$, and $\delta_h = 0.5$ (parallel). The period, T_w of the wave is $1.02\tau_{ce}$ (frequency $f_w = 0.98f_{ce}$).

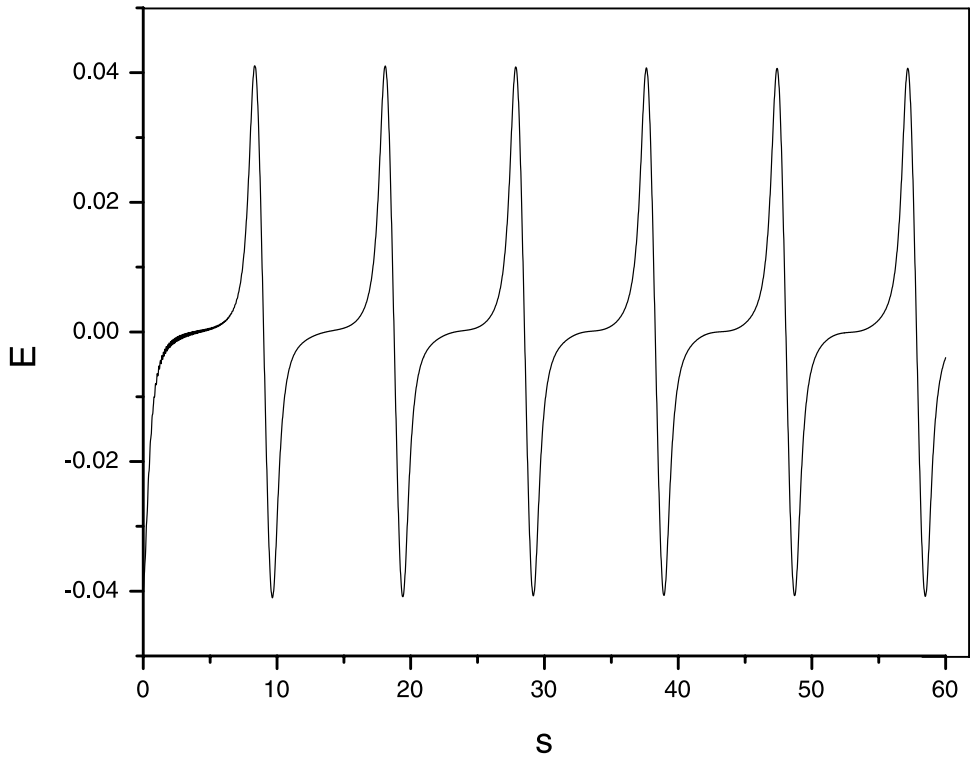

Figure 5a. ESW for varying Mach number, with $E_0 = 0.10$, $\theta = 2°$, $\delta_i = \delta_c = \delta_h = 0.0$, $R_e = 1.0$, $n_{0c}/n_0 = 0.5$, $T_c/T_h = 0.05$, $T_i/T_h = 0.0$, and $M = 2.5$. The period, T_w of the wave is $1.59\tau_{ce}$ (frequency $f_w = 0.63f_{ce}$).

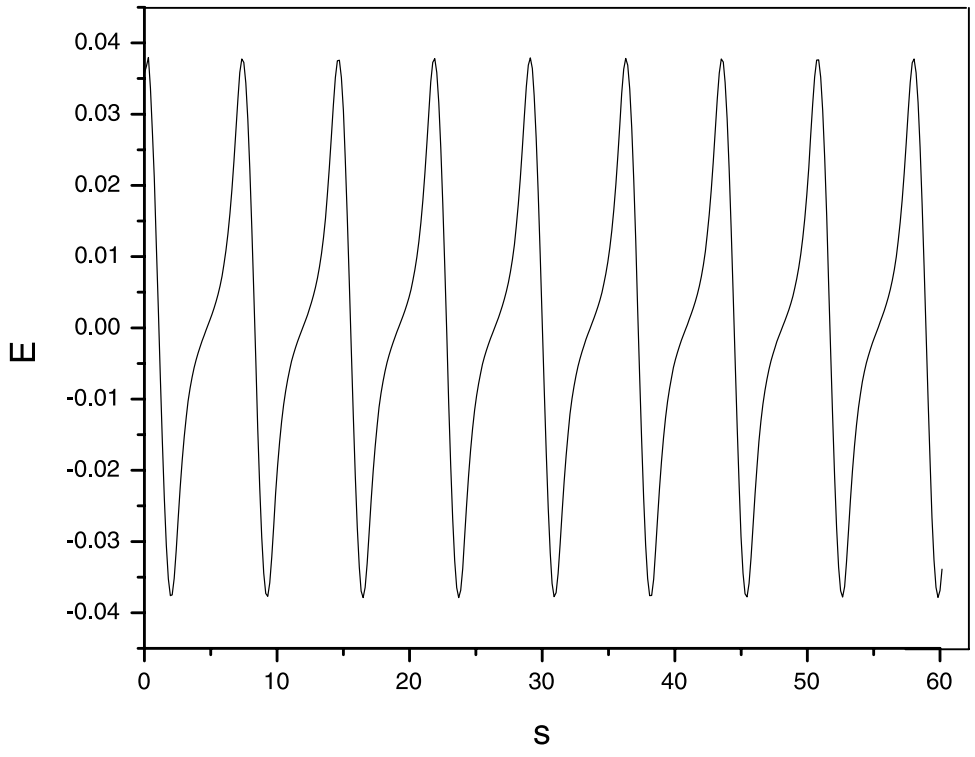

Figure 5b. ESW for varying Mach number, with $E_0 = 0.10$, $\theta = 2°$, $\delta_i = \delta_c = \delta_h = 0.0$, $R_e = 1.0$, $n_{0c}/n_0 = 0.5$, $T_c/T_h = 0.05$, $T_i/T_h = 0.0$, and $M = 2.8$. The period, T_w of the wave is $1.14\tau_{ce}$ (frequency $f_w = 0.88f_{ce}$).

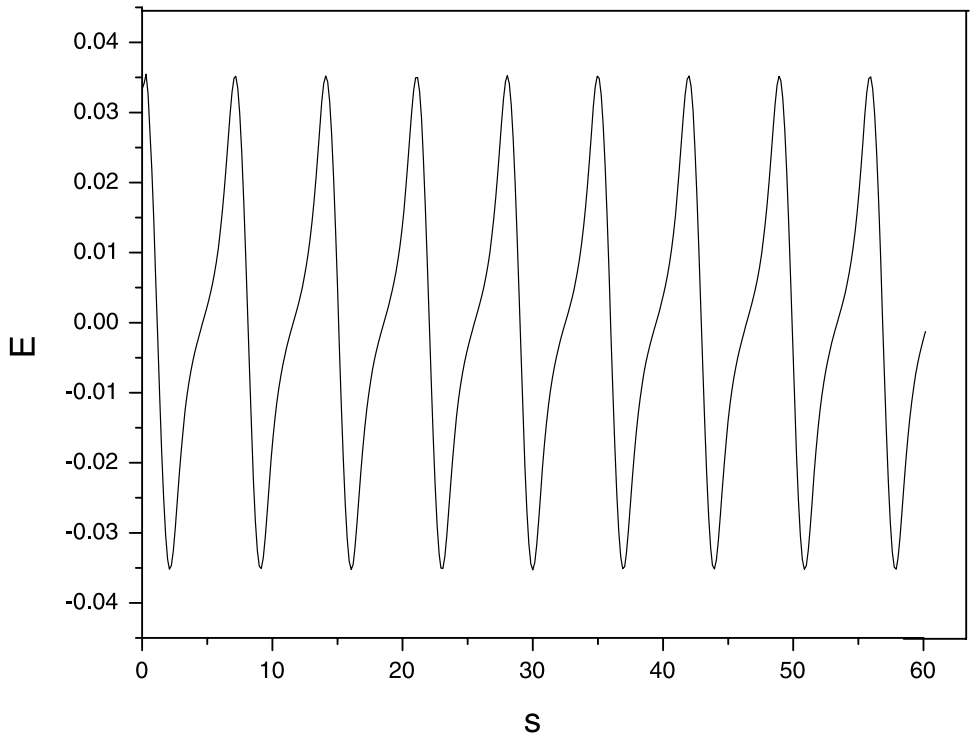

Figure 5c. ESW for varying Mach number, with $E_0 = 0.10$, $\theta = 2°$, $\delta_i = \delta_c = \delta_h = 0.0$, $R_e = 1.0$, $n_{0c}/n_0 = 0.5$, $T_c/T_h = 0.05$, $T_i/T_h = 0.0$, and $M = 3.0$. The period, T_w of the wave is $1.08\tau_{ce}$ (frequency $f_w = 0.93f_{ce}$).

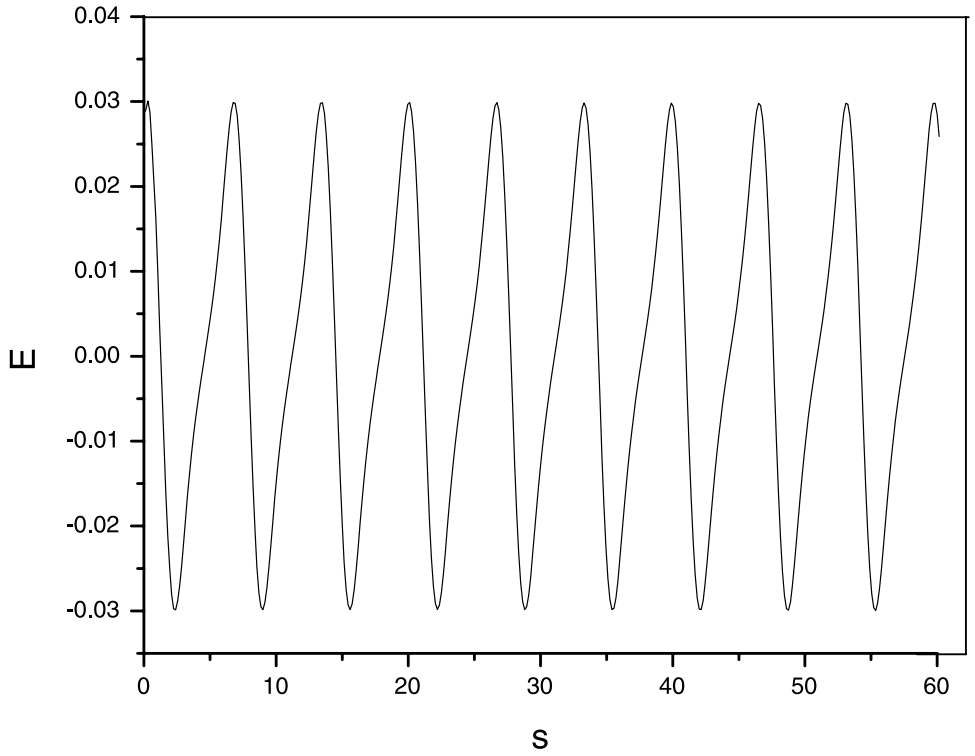

Figure 5d. ESW for varying Mach number, with $E_0 = 0.10$, $\theta = 2°$, $\delta_i = \delta_c = \delta_h = 0.0$, $R_e = 1.0$, $n_{0c}/n_0 = 0.5$, $T_c/T_h = 0.05$, $T_i/T_h = 0.0$, and $M = 3.5$. The period, T_w of the wave is $1.02\tau_{ce}$ (frequency $f_w = 0.98f_{ce}$).

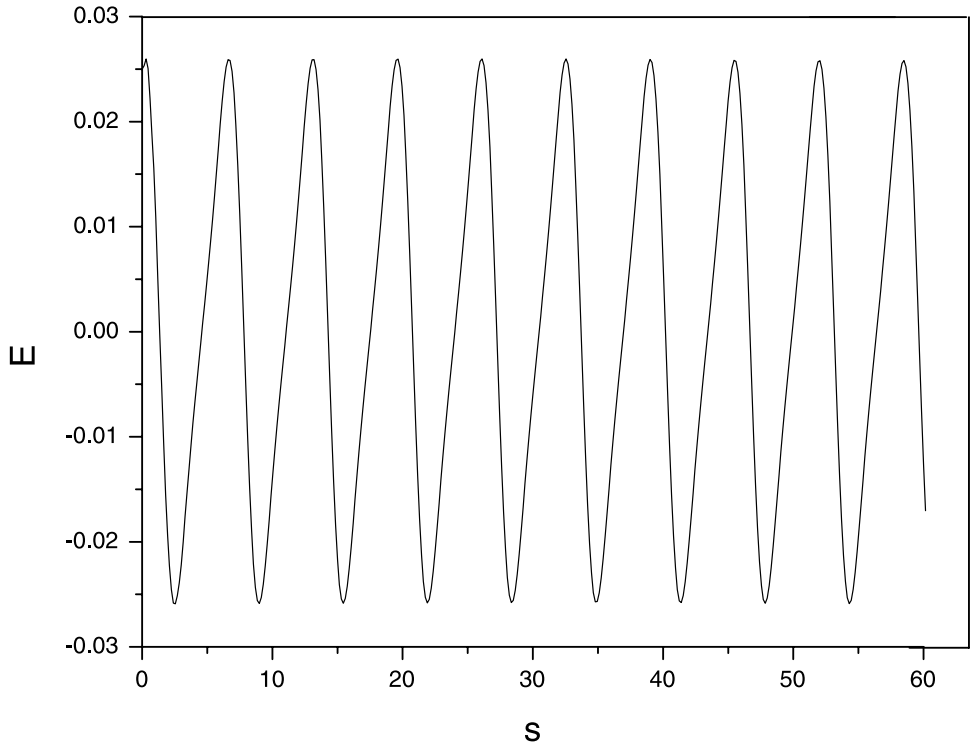

Figure 5e. ESW for varying Mach number, with $E_0 = 0.10$, $\theta = 2^o$, $\delta_i = \delta_c = \delta_h = 0.0$, $R_e = 1.0$, $n_{0c}/n_0 = 0.5$, $T_c/T_h = 0.05$, $T_i/T_h = 0.0$, and $M = 4.0$. The period, T_w of the wave is $0.97\tau_{ce}$ (frequency $f_w = 1.03f_{ce}$).

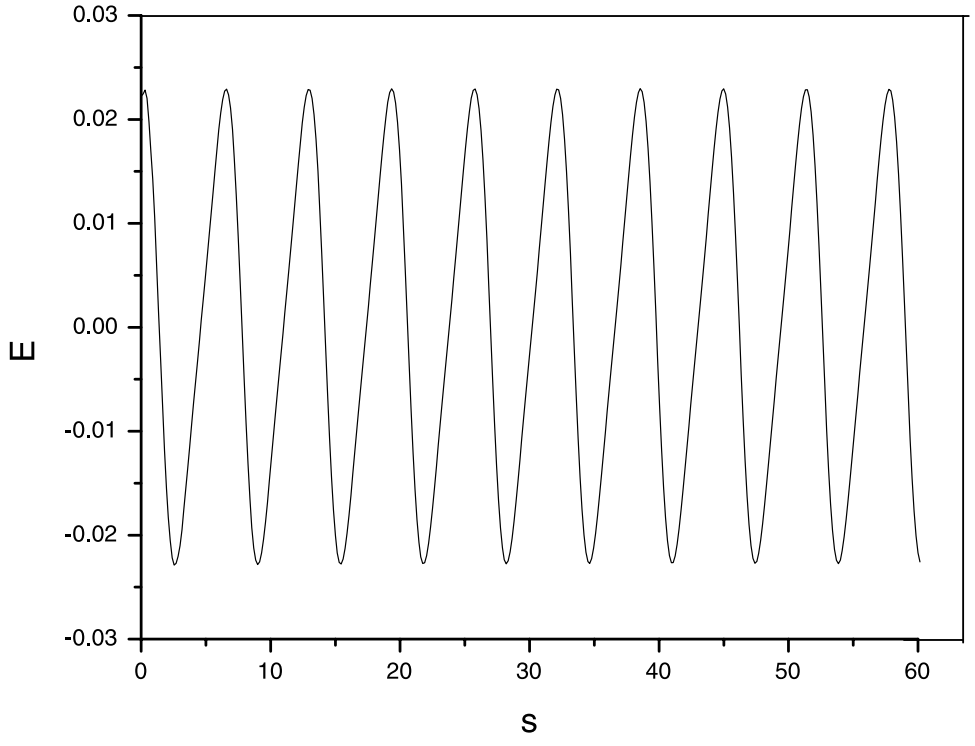

Figure 5f. ESW for varying Mach number, with $E_0 = 0.10$, $\theta = 2^o$, $\delta_i = \delta_c = \delta_h = 0.0$, $R_e = 1.0$, $n_{0c}/n_0 = 0.5$, $T_c/T_h = 0.05$, $T_i/T_h = 0.0$, and $M = 4.5$. The period, T_w of the wave is $0.96\tau_{ce}$ (frequency $f_w = 1.04f_{ce}$).

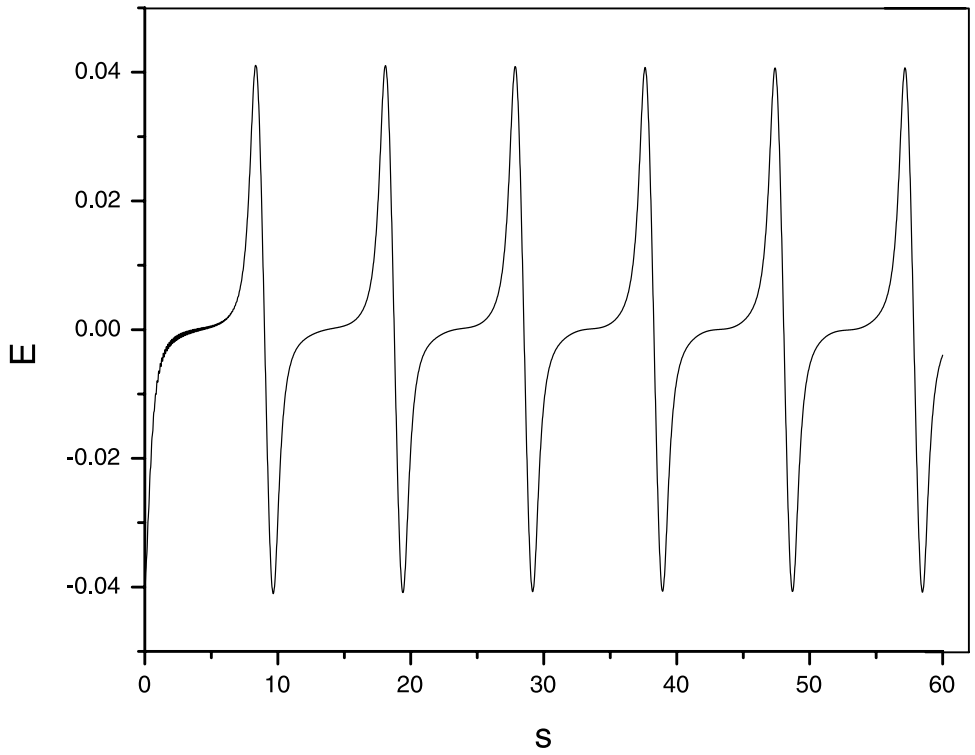

Figure 6a. The electric field corresponding to the fixed parameters $M = 2.5$, $E_0 = 0.10$, $R_e = 1.0$, $\delta_i = \delta_c = \delta_h = 0.0$, $n_{0c}/n_0 = 0.5$, $T_c/T_h = 0.05$, $T_i/T_h = 0.0$, and $\theta = 2^o$.

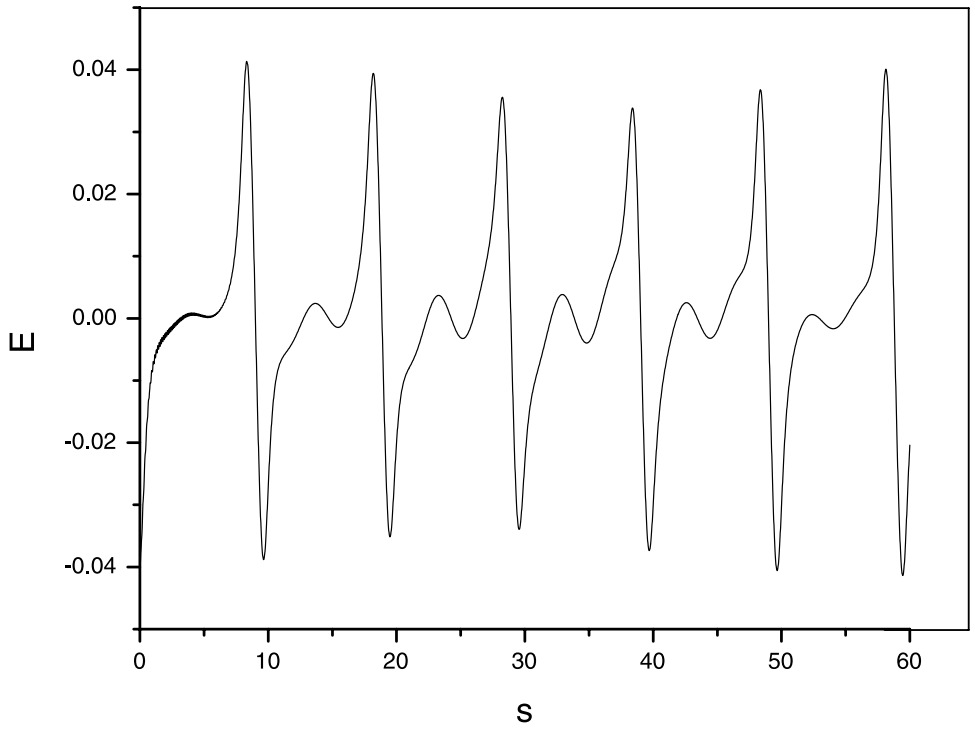

Figure 6b. The electric field corresponding to the fixed parameters $M = 2.5$, $E_0 = 0.10$, $R_e = 1.0$, $\delta_i = \delta_c = \delta_h = 0.0$, $n_{0c}/n_0 = 0.5$, $T_c/T_h = 0.05$, $T_i/T_h = 0.0$, and $\theta = 10^o$.

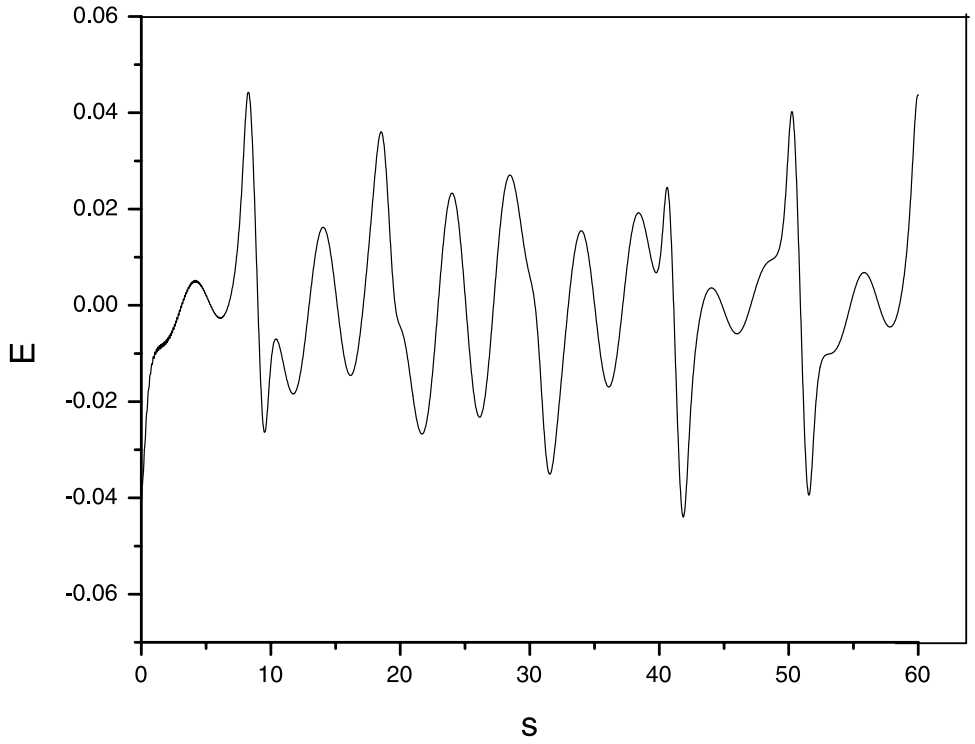

Figure 6c. The electric field corresponding to the fixed parameters $M = 2.5$, $E_0 = 0.10$, $R_e = 1.0$, $\delta_i = \delta_c = \delta_h = 0.0$, $n_{0c}/n_0 = 0.5$, $T_c/T_h = 0.05$, $T_i/T_h = 0.0$, and $\theta = 25^o$.

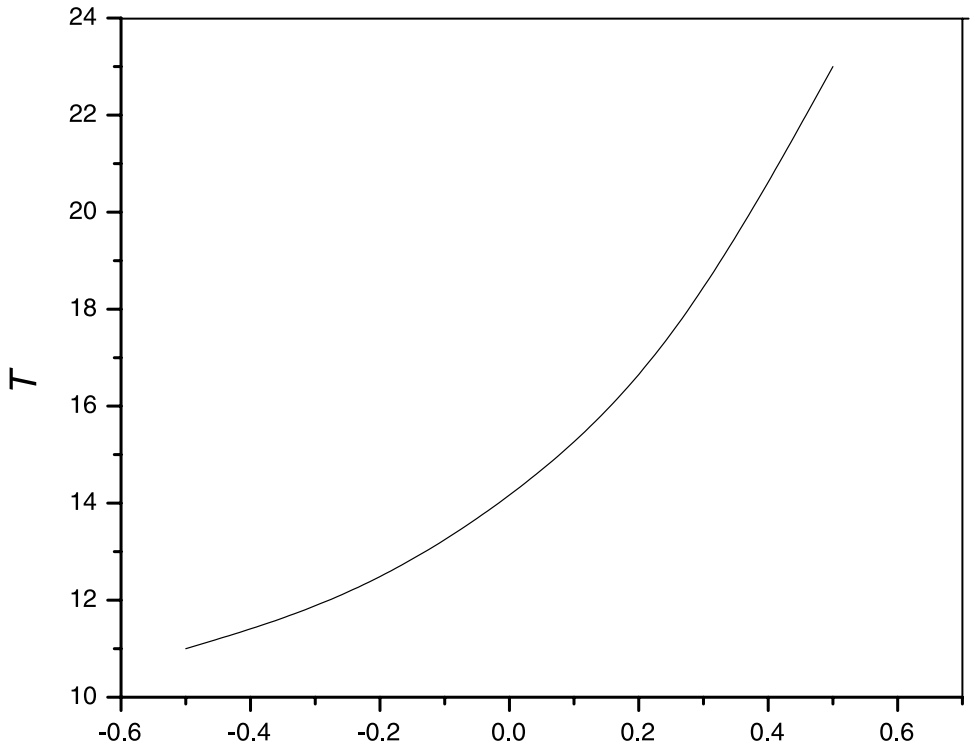

Figure 7a. The period T as a function of the cool electron drift δ_c corresponding to the fixed parameters $M = 2.5$, $E_0 = 0.10$, $R_e = 1.0$, $\delta_i = \delta_h = 0.0$, $n_{0c}/n_0 = 0.5$, $T_c/T_h = 0.05$, $T_i/T_h = 0.0$, and $\theta = 2^o$.

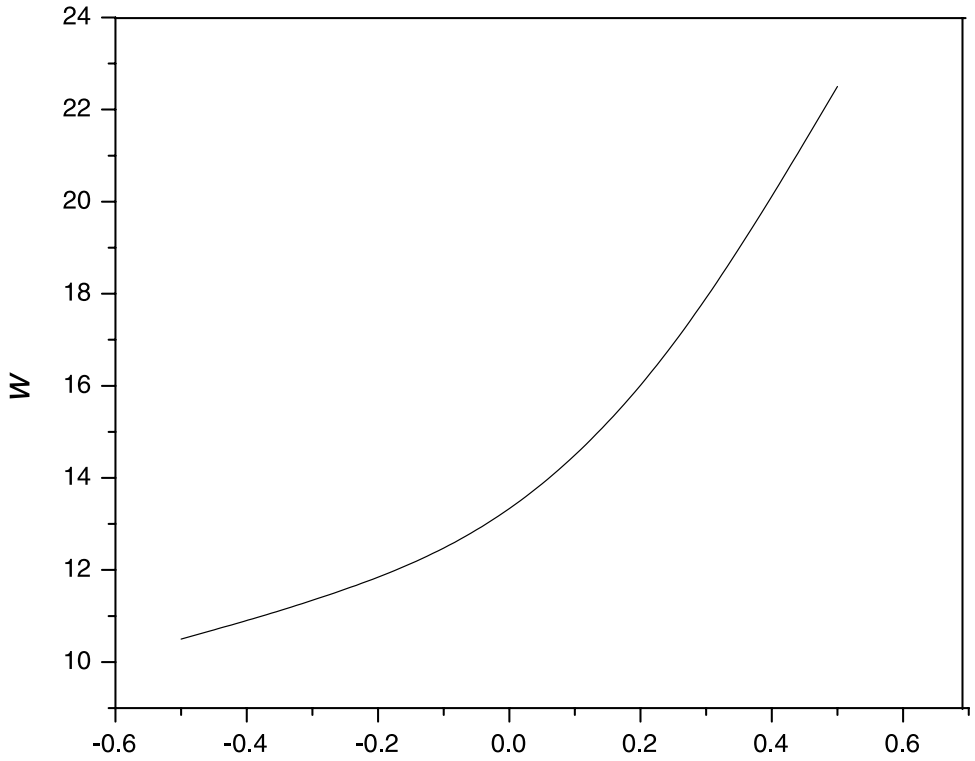

Figure 7b. The pulse width w as a function of the cool electron drift δ_c corresponding to the fixed parameters $M = 2.5$, $E_0 = 0.10$, $R_e = 1.0$, $\delta_i = \delta_h = 0.0$, $n_{0c}/n_0 = 0.5$, $T_c/T_h = 0.05$, $T_i/T_h = 0.0$, and $\theta = 2^o$.

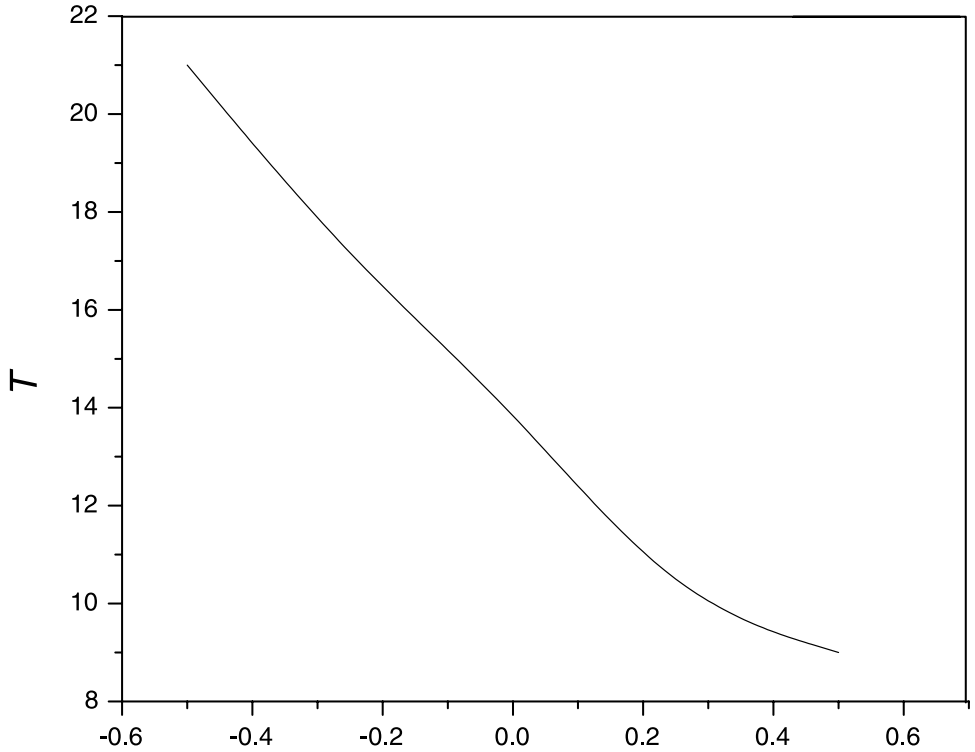

Figure 8a. The period T as a function of the hot electron drift δ_h corresponding to the fixed parameters $M = 2.5$, $E_0 = 0.10$, $R_e = 1.0$, $\delta_i = \delta_c = 0.0$, $n_{0c}/n_0 = 0.5$, $T_c/T_h = 0.05$, $T_i/T_h = 0.0$, and $\theta = 2^o$.

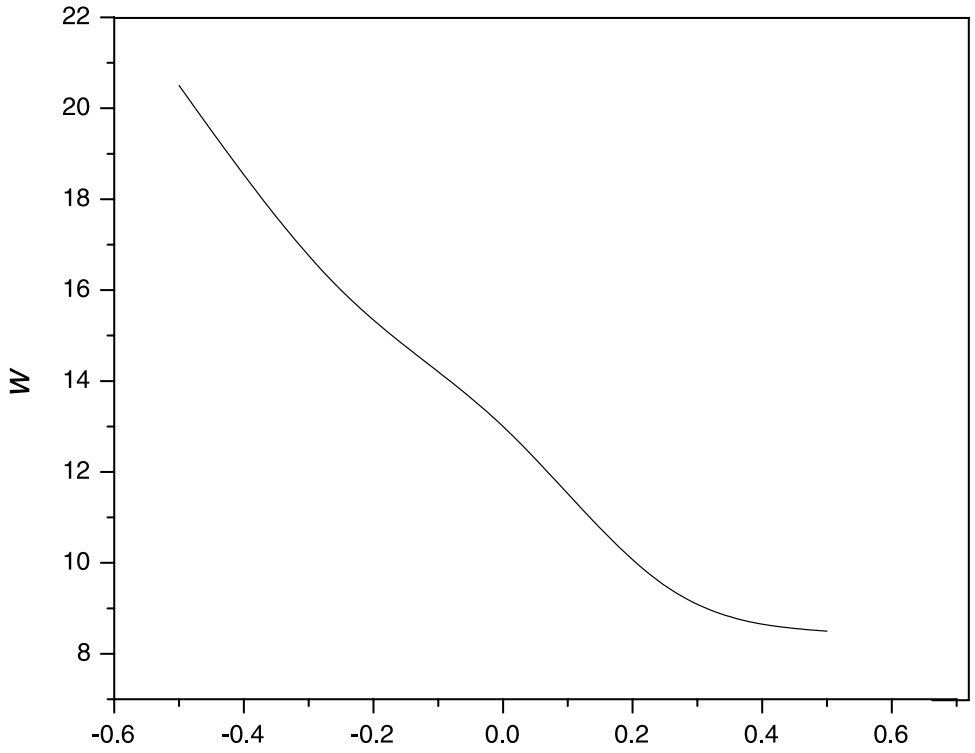

Figure 8b. The pulse width w as a function of the hot electron drift δ_h corresponding to the fixed parameters $M = 2.5$, $E_0 = 0.10$, $R_e = 1.0$, $\delta_i = \delta_c = 0.0$, $n_{0c}/n_0 = 0.5$, $T_c/T_h = 0.05$, $T_i/T_h = 0.0$, and $\theta = 2^o$.

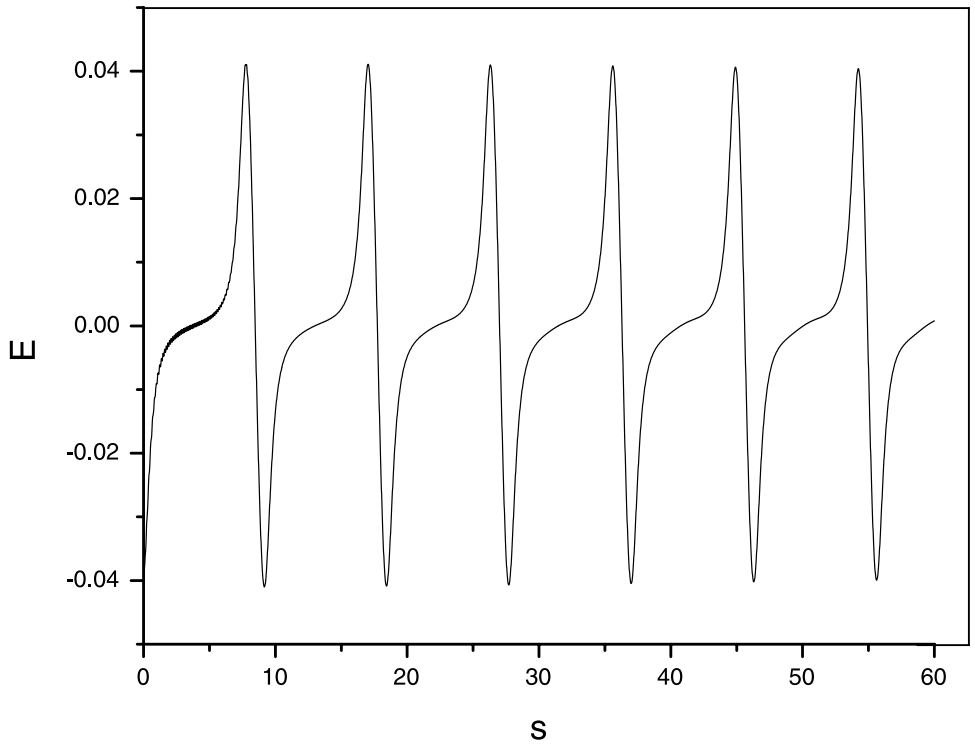

Figure 9a. The electric field corresponding to the fixed parameters $M = 2.5$, $E_0 = 0.10$, $R_e = 1.0$, $\delta_i = \delta_c = \delta_h = 0.0$, $n_{0c}/n_0 = 0.5$, $\theta = 2^o$, $T_i/T_h = 0.0$, and $T_c/T_h = 0.0$. The period, T_w of the wave is $1.48\tau_{ce}$ (frequency $f_w = 0.68f_{ce}$).

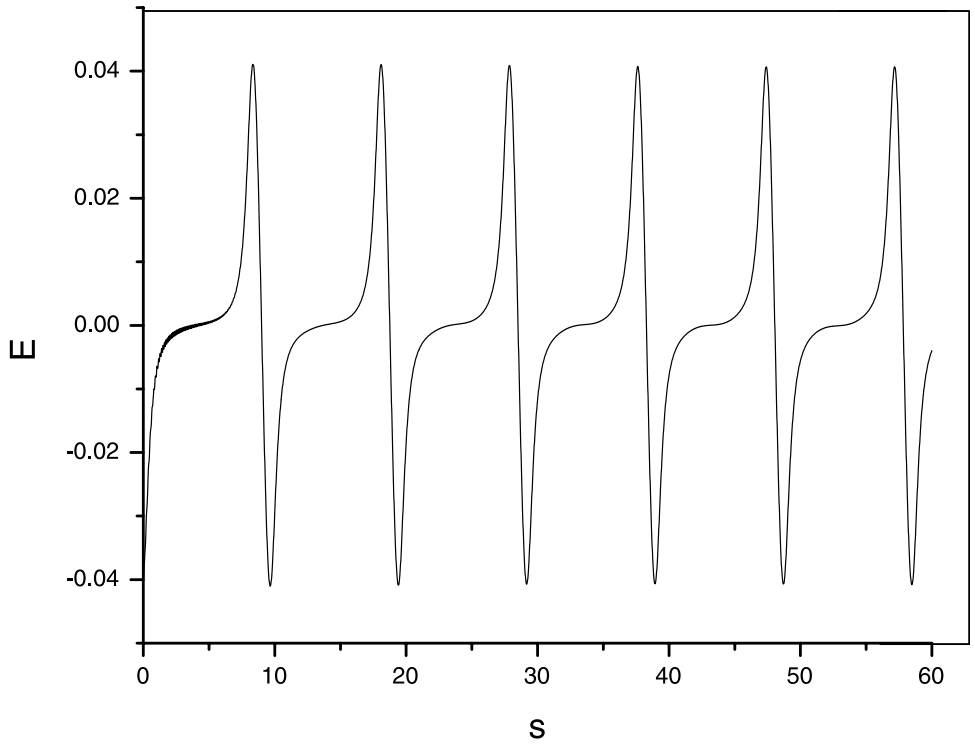

Figure 9b. The electric field corresponding to the fixed parameters $M = 2.5$, $E_0 = 0.10$, $R_e = 1.0$, $\delta_i = \delta_c = \delta_h = 0.0$, $n_{0c}/n_0 = 0.5$, $\theta = 2^o$, $T_i/T_h = 0.0$, and $T_c/T_h = 0.05$. The period, T_w of the wave is $1.59\tau_{ce}$ (frequency $f_w = 0.63f_{ce}$).

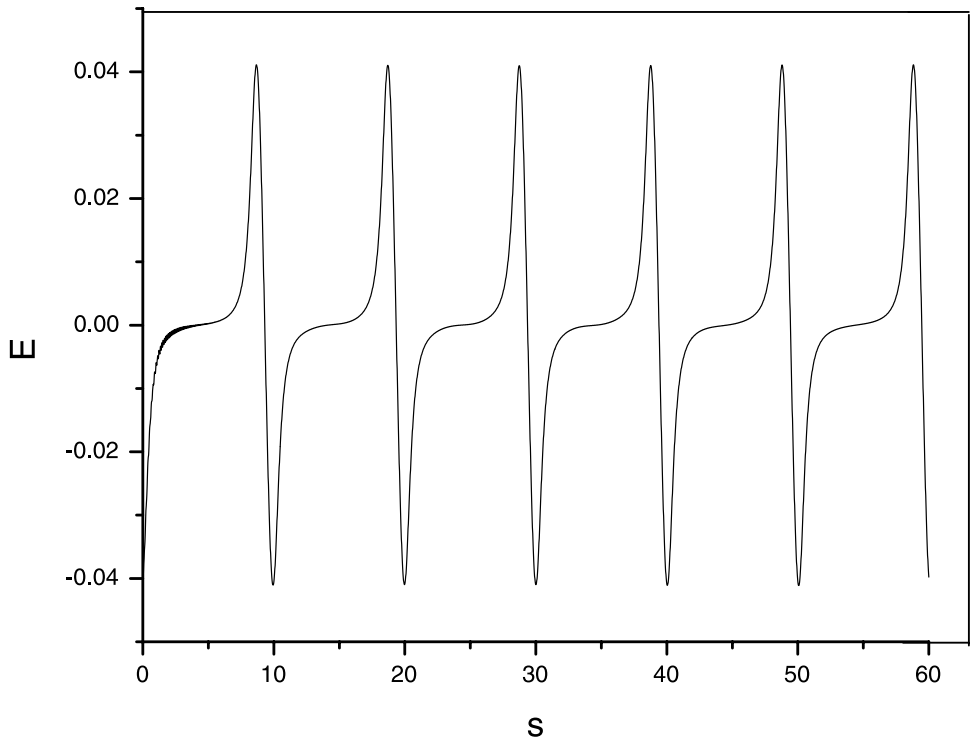

Figure 9c. The electric field corresponding to the fixed parameters $M = 2.5$, $E_0 = 0.10$, $R_e = 1.0$, $\delta_i = \delta_c = \delta_h = 0.0$, $n_{0c}/n_0 = 0.5$, $\theta = 2^o$, $T_i/T_h = 0.0$, and $T_c/T_h = 0.08$. The period, T_w of the wave is $1.65\tau_{ce}$ (frequency $f_w = 0.61f_{ce}$).

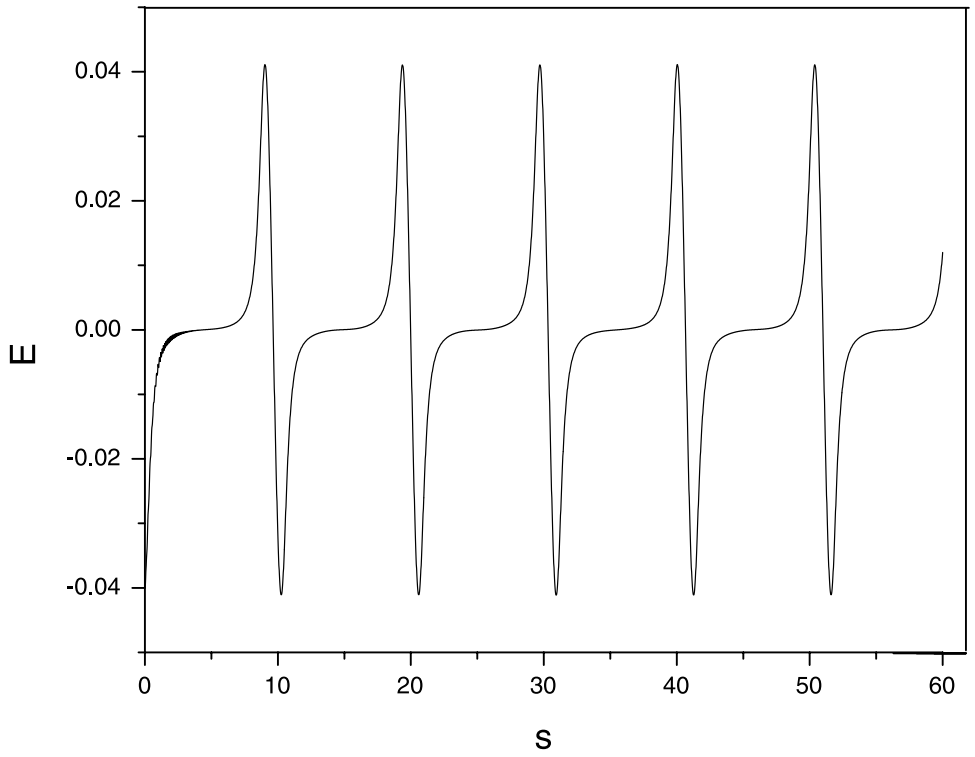

Figure 9d. The electric field corresponding to the fixed parameters M = 2.5, E_0 = 0.10, R_e = 1.0, $\delta_i = \delta_c = \delta_h = 0.0$, $n_{0c}/n_0 = 0.5$, $\theta = 2^o$, $T_i/T_h = 0.0$, and $T_c/T_h = 0.10$. The period, T_w of the wave is $1.71\tau_{ce}$ (frequency $f_w = 0.58f_{ce}$).

3.4. Effect of the Hot Electron Drift

[18] The effect of a drifting hot electron component is seen in Figures 4a–4e. The parameters kept fixed are M = 2.5, $E_0 = 0.10$, $\theta = 2^o$, $n_{0c}/n_0 = 0.5$, $\delta_i = \delta_c = 0.0$, $R_e = 1.0$, $T_c/T_h = 0.05$ and $T_i/T_h = 0.0$. It is seen that motion from an antiparallel to a parallel hot electron drift causes the period of the ESWs to decrease from $2.39\tau_{ce}$ (Figure 4a for $\delta_h = -0.5$) to $1.02\tau_{ce}$ (Figure 4e for $\delta_h = 0.5$). This effect is opposite to that of the cool electron drift which increased the period of the ESWs as one moved from antiparallel to parallel drift. These again represent the EAW since the frequency $\omega < \Omega_e$, and the implication is that the hot electrons are also accelerated in bursts leading to variations in their speeds.

3.5. Effect of Mach Number

[19] Figures 5a–5f show the effect of the Mach number on the ESWs. In these figures, the other fixed parameters are E_0 = 0.10, $\delta_i = \delta_c = \delta_h = 0.0$, $n_{0c}/n_0 = 0.5$, $T_c/T_h = 0.05$, $T_i/T_h = 0.0$, $\theta = 2^\circ$, and $R_e = 1.0$, while M is varied from 2.5 (Figure 5a) to 4.5 (Figure 5f). It is seen that as M increases, the nonlinearity of the electric field is suppressed. This means that the electric field needs to be driven more strongly to become nonlinear (i.e., E_0 needs to be increased). This would however give unrealistically high amplitudes which would not correspond to the satellite observations. Hence for a Mach number of 2.5 (the minimum value for which the waveforms exist), an E_0 value of 0.1 shows nonlinearity. Also, the period of the ESWs decreases as M increases, as well as the suppression in nonlinearity. For M = 2.5, the period of the ESW is $1.59\tau_{ce}$, which decreases to $0.96\tau_{ce}$ for M = 4.5. Conversely, the frequency increases from $0.63f_{ce}$ for M = 2.5 to $1.04f_{ce}$ for M = 4.5.

3.6. Effect of Propagation Angle

[20] Figures 6a–6c show the effect of the propagation angle on the ESWs. In these figures, the other fixed parameters are M = 2.5, E_0 = 0.10, $\delta_i = \delta_c = \delta_h = 0.0$, $n_{0c}/n_0 = 0.5$, $T_c/T_h = 0.05$, $T_i/T_h = 0.0$, and $R_e = 1.0$, while θ is varied from 2° (Figure 6a) to 25° (Figure 6c). For a propagation angle of 10^o, there is evidence of a slight distortion of the ESW with fluctuations in amplitude. This figure shows a very close resemblance to the TYPE C BEN waveforms observed by *Matsumoto et al.* [1994], with its double-humped continuous appearance. A comparison of our Figure 6 with the observations of *Matsumoto et al.* [1994] reveals that as the propagation angle of the wave increases relative to the ambient magnetic field, the nonlinear electric-field structures transform from a uniform TYPE A BEN waveform to a more distorted TYPE C waveform. For values of $\theta > 10^\circ$, the ESWs were found to lose structure and develop into random numerical noise. Our findings appear to confirm the experimental observations made by the POLAR [*Franz et al.*, 1998] and GEOTAIL [*Matsumoto et al.*, 1994] spacecrafts showing that the ESWs are observed in a narrow cone about the direction of the magnetic field.

3.7. Study of the ESW Period (T) and Pulse Width (w)

[21] The relationship between the ESW period (T) and pulse width (w) as a function of the cool and hot electron

flow velocities, $\delta_c = v_{0c}/v_{th}$ and $\delta_h = v_{0h}/v_{th}$, respectively, was also examined. Figures 7a and 7b show that both T and w increase, as the normalized cool electron flow velocity δ_c increases. From the figures we find that $w/T \approx 0.9$. A similar behavior has been reported from satellite observations by *Kojima et al.* [1994]. In their measurements they found that for a variety of ESWs, the ratio of w/T was constant, with $w/T = 0.3$ [see *Kojima et al.*, 1994, Figure 3]. The hot electron flow velocity has the opposite effect on the period and pulse width of the ESWs. From Figures 8a and 8b, it is seen that the period and pulse width decrease as δ_h increases; however, the ratio of the period to the pulse width T/w remains unchanged at 0.9.

3.8. Effect of Cool Electron Temperature on the ESWs

[22] Figure 9 shows the effect of a finite cool electron temperature on the waves, with other parameters fixed: $M = 2.5$, $E_0 = 0.10$, $\theta = 2°$, $\delta_i = \delta_c = \delta_h = 0.0$, $n_{0c}/n_0 = 0.5$, $T_i/T_h = 0.0$, and $R_e = 1.0$. An increase in the cool electron temperature is seen to result in a broadening of the waves, with an increase in the period and nonlinearity. The period increases from $1.48\tau_{ce}$ for $T_c/T_h = 0.0$ to $1.71\tau_{ce}$ for $T_c/T_h = 0.10$. Similar studies for the cool ion temperature showed no effect on the ESWs.

4. Conclusion

[23] In this paper we have explored the theoretical model proposed by *Moolla et al.* [2003], conducting a detailed study of nonlinear waveforms similar to those observed by the POLAR [*Franz et al.*, 1998] and GEOTAIL [*Matsumoto et al.*, 1994] spacecrafts in the high-frequency component of BEN. As explained in the earlier work, the high-frequency nonlinear structures arise from two linear modes, the electron cyclotron wave (ECW) and the electron acoustic wave (EAW) that couple via convective derivatives in the fluid equations. In particular, we have investigated the relationship between pulse widths and periods of the ESWs and showed that their ratio w/T is constant, confirming the experimental observations of *Kojima et al.*, 1994]. We have also showed that for higher propagation angles, the shape of the waveforms transform from the uniform TYPE A BEN-like structures to a more distorted, double-humped TYPE C BEN-like shapes. The effect of finite cool electron temperature was found to broaden the waves and increase the nonlinearity. The unnormalized electric field is given as

$$E_{UN} = -\frac{\partial\phi}{\partial x} = \frac{\Omega_e}{V}\frac{\partial\phi}{\partial s} = \frac{\Omega_e}{Mv_{th}}T_h/e\frac{\partial\psi}{\partial s} = \frac{E}{M}\frac{T_h}{e\rho_e} \qquad (20)$$

For the spiky structures obtained in this paper, for T_h varying from 10 eV to 100 eV and for a magnetic field of about 13000 nT, equation (23) predicts amplitudes in the range from about 670 mV/m to a few V/m. The amplitude of the parallel electric field observed by the FAST satellite [*Ergun et al.*, 1998] is about 700 mV/m, which is within the predicted range of values.

[24] **Acknowledgments.** We acknowledge support from the NRF, South-Africa-India Bilateral Programme. SM would like to thank the IIG, Mumbai for his visit during which this paper was finalized. GSL would like to thank the council of Scientific and Industrial Research (CSIR), Government of India, for support under the Emeritus Scientist Scheme.

[25] Amitava Bhattacharjee thanks the reviewers for their assistance in evaluating this paper.

References

Anderson, R. R., C. C. Harvey, M. M. Hoppe, B. T. Tsurutani, T. E. Eastman, and J. Etcheto (1982), Plasma waves near the magnetopause, *J. Geophys. Res.*, 2087.

Berthomier, M., R. Pottellette, and M. Malingre (1998), Solitary waves and weak double layers in a two-electron temperature auroral plasma, *J. Geophys. Res.*, *103*, 4261.

Berthomier, M., R. Pottellette, M. Malingre, and Y. Khotyaintsev (2000), Electron-acoustic solitons in an electron-beam plasma system, *Phys. Plasmas*, *7*, 2987.

Bostrom, R., G. Gustafsson, B. Holback, G. Holmgren, H. Koskinen, and P. Kintner (1988), Characteristics of solitary waves and weak double layers in the magnetospheric plasma, *Phys. Rev. Lett.*, *61*, 82.

Dubouloz, N., R. Pottelette, M. Malingre, and R. A. Treumann (1991a), Generation of broadband electrostatic noise by electron acoustic solitons, *Geophys. Res. Lett.*, *18*, 155.

Dubouloz, N., R. Pottelette, M. Malingre, G. Holmgren, and P. A. Lindqvist (1991b), Detailed analysis of broadband electrostatic noise in the dayside auroral zone, *J. Geophys. Res.*, *96*, 3565.

Dubouloz, N., R. A. Treumann, R. Pottelette, and M. Malingre (1993), Turbulence generated by a gas of electron acoustic solitons, *J. Geophys. Res.*, *98*, 17,415.

Ergun, R. E., et al. (1998), FAST satellite observations of electric field structures in the auroral zone, *Geophys. Res. Lett.*, *25*, 2025.

Franz, J. R., P. M. Kintner, and J. S. Pickett (1998), POLAR observations of coherent electric field structures, *Geophys. Res. Lett.*, *25*, 1277.

Goldman, M. V., M. Oppenheim, and D. L. Newman (1999), Nonlinear two-stream instabilities as an explanation for auroral bipolar wave structures, *Geophys. Res. Lett.*, *26*, 1821.

Goldman, M. V., F. Crary, D. L. Newman, and M. Oppenheim (2000), Turbulence driven by two-stream instability in a magnetized plasma, *Phys. Plasmas*, *7*, 1732.

Gurnett, D. A., and L. A. Frank (1977), A region of intense plasma wave turbulence on auroral field lines, *J. Geophys. Res.*, *82*, 1031.

Gurnett, D. A., and L. A. Frank (1978), Plasma waves in the polar cusp: Observations from Hawkeye 1, *J. Geophys. Res.*, *83*, 1447.

Gurnett, D. A., R. R. Anderson, and B. T. Tsurutani (1979), Plasma waves at the magnetopause: Observations from ISEE 1 and 2, *J. Geophys. Res.*, *84*, 7043.

Kojima, H., et al. (1994), Relation between electrostatic solitary waves and hot plasma flow in the plasma sheet boundary layer: Geotail observations, *Geophys. Res. Lett.*, *21*, 2919.

Kojima, H., H. Matsumoto, S. Chikuba, S. Horiyama, M. Ashour-Abdalla, and R. R. Anderson (1997), Geotail waveform observations of broadband/narrowband electrostatic noise in the distant tail, *J. Geophys. Res.*, *102*, 14,439.

Kojima, H., Y. Omura, H. Matsumoto, K. Miyaguti, and T. Mukai (1999), Characteristics of electrostatic solitary waves observed in the plasma sheet boundary: Statistical analyses, *Nonlinear Processes Geophys.*, *6*, 179.

Koskinen, H., R. Lundin, and B. Holback (1990), On the plasma environment of solitary waves and weak double layers, *J. Geophys. Res.*, *95*, 5921.

Krasovsky, V. L., H. Matsumoto, and Y. Omura (1997), Bernstein-Greene-Kruskal analysis of electrostatic solitary waves observed with Geotail, *J. Geophys. Res.*, *102*, 22.

Krasovsky, V. L., H. Matsumoto, and Y. Omura (2004), On the three-dimensional configuration of electrostatic solitary waves, *Nonlinear Processes Geophys.*, *11*, 313.

LaBelle, J., and R. A. Treumann (1998), Plasma waves at the dayside magnetopause, *Space Sci. Rev.*, *47*, 175.

Lakhina, G. S., and B. T. Tsurutani (1999), A generation mechanism for the polar cap boundary layer broadband plasma waves, *J. Geophys. Res.*, *104*, 279.

Lakhina, G. S., B. T. Tsurutani, H. Kojima, and H. Matsumoto (2000), Broadband plasma waves in the boundary layers, *J. Geophys. Res.*, *105*, 27,791.

Lakhina, G. S., B. T. Tsurutani, S. V. Singh, and R. V. Reddy (2003), Some theoretical models for solitary structures of boundary layer waves, *Nonlinear Processes Geophys.*, *10*, 65.

Mace, R. L., and M. Hellberg (1993), Electron-acoustic and cyclotron-sound instabilities driven by field-aligned hot electron streaming, *J. Geophys. Res.*, *98*, 5881.

Matsumoto, H., H. Kojima, T. Miyatake, Y. Omura, M. Okada, I. Nagano, and M. Tsutsui (1994), Electrostatic solitary waves (ESW) in the magnetotail: BEN wave forms observed by Geotail, *Geophys. Res. Lett.*, *21*, 2915.

Moolla, S., R. Bharuthram, S. V. Singh, and G. S. Lakhina (2003), Nonlinear high-frequency waves in the magnetosphere, *PRAMANA J. Phys.*, *61*, 1209.

Mozer, F. S., R. E. Ergun, M. Temerin, C. Cattell, J. Dombeck, and J. Wygant (1997), New features of time domain electric-field structures in the auroral acceleration region, *Phys. Rev. Lett.*, *79*, 1281.

Muschietti, L., R. E. Ergun, I. Roth, and C. W. Carlson (1999), Phase-space electron holes along magnetic field lines, *Geophys. Res. Lett.*, *26*, 1093.

Omura, Y., H. Kojima, and H. Matsumoto (1994), Computer simulation of electrostatic solitary waves: A nonlinear model of broadband electrostatic noise, *Geophys. Res. Lett.*, *21*, 2923.

Omura, Y., H. Matsumoto, T. Miyatake, and H. Kojima (1996), Electron beam instabilities as generation mechanism of electrostatic solitary waves in the magnetotail, *J. Geophys. Res.*, *101*, 2685.

Omura, Y., H. Kojima, N. Miki, T. Mukai, H. Matsumoto, and R. R. Anderson (1999), Electrostatic solitary waves carried by diffused electron beams observed by the Geotail spacecraft, *J. Geophys. Res.*, *104*, 14,627.

Pickett, J. S., et al. (2004), Solitary waves observed in the auroral zone: The Cluster multi-spacecraft perspective, *Nonlinear Processes Geophys.*, *11*, 183.

Press, W. H., S. A. Teukolsky, W. T. Vetterling, and B. P. Flannery (1996), *Numerical Recipes in Fortran 90—The Art of Parallel Scientific Computing*, Cambridge Univ. Press, New York.

Reddy, R. V., and G. S. Lakhina (1991), Ion acoustic double layers and solitons in auroral plasma, *Planet. Space Sci.*, *39*, 1343.

Reddy, R. V., G. S. Lakhina, and F. Verheest (1992), Ion-acoustic double layers and solitons in multispecies auroral beam plasmas, *Planet. Space Sci.*, *40*, 1055.

Reddy, R. V., G. S. Lakhina, N. Singh, and R. Bharuthram (2002), Spiky parallel electrostatic ion cyclotron and ion acoustic waves, *Nonlinear Processes Geophys.*, *9*, 25.

Schriver, D., and M. Ashour-Abdalla (1987), Generation of high-frequency broadband electrostatic noise—The role of cold electrons, *J. Geophys. Res.*, *92*, 5807.

Singh, N. (2003), Space-time evolution of electron-beam driven electron holes and their effects on the plasma, *Nonlinear Processes Geophys.*, *10*, 53.

Singh, S. V., and G. S. Lakhina (2001), Generation of electron-acoustic waves in the magnetosphere, *Planet. Space Sci.*, *49*, 107.

Singh, S. V., R. V. Reddy, and G. S. Lakhina (2001a), Broadband electrostatic noise due to nonlinear electron-acoustic waves, *Adv. Space Res.*, *28*, 111,643.

Singh, S., S. M. Loo, B. E. Wells, and G. S. Lakhina (2001b), Evolution of electron beam generated waves resulting in transverse ion heating and filamentation of the plasma, *J. Geophys. Res.*, *106*, 21,165.

Temerin, M., M. Woldorff, and F. S. Mozer (1979), Nonlinear steepening of the electrostatic ion cyclotron wave, *Phys. Rev. Lett.*, *43*, 1941.

Temerin, M., K. Cerny, W. Lotko, and F. S. Mozer (1982), Observations of double layers and solitary waves in the auroral plasma, *Phys. Rev. Lett.*, *48*, 1175.

Tsurutani, B. T., E. J. Smith, R. M. Thorne, R. R. Anderson, D. A. Gurnett, G. K. Parks, C. C. Lin, and C. T. Russell (1981), Wave-particle interactions at the magnetopause: Contributions to the dayside aurora, *Geophys. Res. Lett.*, *8*, 183.

Tsurutani, B. T., A. L. Brinca, E. J. Smith, R. T. Okida, R. R. Anderson, and T. E. Eastman (1989), A statistical study of ELF-VLF plasma waves at the magnetopause, *J. Geophys. Res.*, *94*, 1270.

Tsurutani, B. T., G. S. Lakhina, C. M. Ho, J. K. Arballo, C. Galvan, A. Boonsiriseth, J. S. Pickett, D. A. Gurnett, W. K. Peterson, and R. M. Thorne (1998a), Broadband plasma waves observed in the polar cap boundary layer: Polar, *J. Geophys. Res.*, *103*, 17,351.

Tsurutani, B. T., J. K. Arballo, G. S. Lakhina, C. M. Ho, B. Buti, J. S. Pickett, and D. A. Gurnett (1998b), Plasma waves in the dayside polar cap boundary layer: Bipolar and monopolar electric pulses and whistler mode waves, *Geophys. Res. Lett.*, *25*, 4117.

R. Bharuthram, University of Witwatersrand, Wits 2050, Johannesburg, South Africa.

G. S. Lakhina, R. V. Reddy, and S. V. Singh, Indian Institute of Geomagnetism, New Panvel (West), Navi Mumbai, 410218, India.

S. Moolla, Department of Physics, University of Kwa-Zulu Natal, Westville Campus, Private Bag X54001, Durban 4000, South Africa. (moollas@ukzn.ac.za)